






RESEARCH ARTICLE | OCTOBER 25 2023

## Control of acoustic scattering of trailing edge flow by distributed compliance

Irsalan Arif ; Muhammad Rehan Naseer ; Randolph C. K. Leung  ; Shuaib Salamat 



*Physics of Fluids* 35, 106115 (2023)

<https://doi.org/10.1063/5.0165765>



### Articles You May Be Interested In

A computational study of trailing edge noise suppression with embedded structural compliance

*JASA Express Lett.* (February 2023)

Distributed surface compliance for airfoil tonal noise reduction at various loading conditions

*Physics of Fluids* (April 2022)

Suppression of deep cavity aeroacoustics at low Mach number by localized surface compliance

*Physics of Fluids* (May 2023)



Physics of Fluids

## Special Topics Open for Submissions

[Learn More](#)

# Control of acoustic scattering of trailing edge flow by distributed compliance

Cite as: Phys. Fluids **35**, 106115 (2023); doi: [10.1063/5.0165765](https://doi.org/10.1063/5.0165765)

Submitted: 30 June 2023 · Accepted: 5 October 2023 ·

Published Online: 25 October 2023



View Online



Export Citation



CrossMark

Irsalan Arif,<sup>1,2</sup> Muhammad Rehan Naseer,<sup>1</sup> Randolph C. K. Leung,<sup>1,a)</sup> and Shuaib Salamat<sup>2</sup>

## AFFILIATIONS

<sup>1</sup>Department of Mechanical Engineering, The Hong Kong Polytechnic University, Hong Kong, People's Republic of China

<sup>2</sup>Department of Aerospace Engineering, College of Aeronautical Engineering, National University of Sciences and Technology, Islamabad, Pakistan

<sup>a)</sup> Author to whom correspondence should be addressed: [mmrleung@polyu.edu.hk](mailto:mmrleung@polyu.edu.hk)

## ABSTRACT

In this paper, an approach for the reduction of trailing edge noise due to flow scattering from a semi-infinite splitter plate is proposed. It utilizes the fluid–structure interactions of well-designed multiple compliant elastic panels to suppress the flow instabilities within the boundary layers over the splitter plate to reduce overall trailing edge noise scattering. The approach is studied numerically using high-fidelity direct aeroacoustic simulation at low Reynolds numbers based on a panel length of  $5 \times 10^4$ . The noise reduction efficacy of the approach is analyzed by studying two different cases, and their underlying physical mechanisms are explored. First, the boundary layer over one side of the plate is subjected to a weak monochromatic acoustic excitation to produce laminar instabilities. Second, the boundary layer is subjected to a weak broadband excitation within the boundary layer. For each case, the panel system is uniquely designed with thorough consideration of the flow characteristics of the boundary layer instabilities of the problem. Comprehensive aeroacoustic analyses reveal that a significant sound power level reduction of 4.2 and 7.4 dB can be achieved by designed configurations for both kinds of excitation without any drag penalty. Nonlinear fluid–structure interactions of carefully designed elastic panels result in a weak correlation between the near-field flow instabilities and far-field noise. The flow-induced panel structural resonance is proven to effectively absorb the energy of boundary layer instabilities and their scattering at the trailing edge. Key characteristics for the design of compliance systems under different flow conditions are discerned and discussed.

Published under an exclusive license by AIP Publishing. <https://doi.org/10.1063/5.0165765>

## I. INTRODUCTION

Trailing edge noise is one of the most fundamental source mechanisms, which is associated with many engineering applications including wind turbines, fixed and rotating blades, rotors, and fans.<sup>1–3</sup> It is generally produced by the interaction of boundary layer instabilities with the sharp trailing edge of a rigid structure which eventually scatters as acoustic waves.<sup>4,5</sup> It is widely recognized as one of the key factors that limit the operational capabilities and sustainable design of these engineering systems. The phenomenon of trailing edge noise and its underlying principles have been well studied in several experimental and numerical investigations.<sup>2,3,6,7</sup>

Over the years, a number of strategies have been proposed and tested to achieve trailing edge noise reduction. Some of these include the modification of trailing edge geometry such as serrations,<sup>8–10</sup> flap-lets,<sup>11,12</sup> extensions,<sup>13,14</sup> brushes,<sup>15</sup> and bio-inspired structures<sup>16,17</sup> and application of porous structures for trailing edge noise control.<sup>18–24</sup> Utilization of structural elasticity for trailing edge noise control has

also been explored in recent times. The effect of compliant trailing edges was first studied by Crighton and Leppington,<sup>25</sup> who analyzed the acoustic scattering by a semi-infinite compliant plate using the Wiener–Hopf method. They identified that the radiated intensity had a direct relation with sixth-power flow velocity under heavy fluid loading. Howe<sup>26</sup> studied the noise scattering of a semi-infinite elastic plate analytically for a turbulent boundary layer and showed that an elastic plate produced much lower acoustic radiation by trailing edge scattering under heavy fluid loading. However, the structural bending waves of the elastic structure resulted in an increase in noise at lower frequencies. Manela<sup>27</sup> in his analytical study claimed that the motion of an elastic trailing edge can affect the noise radiation characteristics. Jaworski and Peake<sup>20</sup> also analyzed the effects of structural elasticity on noise reduction for a semi-infinite poroelastic plate and observed that the noise reduction by the flexible trailing edge was found to be dependent on the structural frequency. Later, Cavalieri *et al.*<sup>21</sup> analyzed the characteristics of a finite elastic cantilever plate numerically and

showed that the noise radiation is amplified at the resonant frequencies of the structure. Ayton<sup>22</sup> analytically investigated a similar configuration to analyze the noise radiation by poroelastic extension by the Wiener–Hopf method and observed the noise reduction characteristics by elastic plates. Later, Colbrook and Ayton<sup>28</sup> showed the benefits of using small trailing edge extensions in noise control for mid- to high-frequency range.

With recent advancements in computational technologies, noise control methods based on the fluid–structure interactions induced by the presence of structural compliance have also been attempted by extensive numerical investigations. Bae *et al.*<sup>29</sup> conducted a numerical investigation of the aeroacoustics characteristics of a splitter plate with an elastic cantilever extension and observed noise reduction as well as amplification at the elastic plate's natural frequency. A comprehensive numerical study of Nardini *et al.*<sup>30</sup> for a similar configuration involving external excitation showed some noise reduction/amplification depending on the relative amplitude and phase of the incident flow unsteadiness and edge structural motion. Recently, Serrano-Galiano *et al.*<sup>31</sup> and Kolb and Schaefer<sup>32</sup> also studied the aeroacoustics of the full membrane airfoil/plate. Their results indicate that a fully elastic structure can effectively delay the occurrence of stall, but it is ineffective in noise reduction and leads to noise amplification at certain flow conditions.

The aforementioned studies have analyzed the aeroacoustics characteristics of the elastic structures along with their potential in trailing edge noise reduction; however, the design requirements of the elastic panel/membranes are not discussed. Hence, it remains unclear on how to achieve optimal noise reduction by using fluid–structure interactions of elastic panels/membranes or how to design/modify the existing structures based on the operating conditions of the device. Furthermore, the existing utilization of an elastic structure is limited to trailing edges only which makes the overall system a cantilever structure. Hence, the overall structural integrity of the system becomes questionable as these structures may experience aeroelastic divergence or flutter in certain operating conditions.<sup>33</sup> These undesirable side effects not only result in extra vibroacoustic sources for noise amplification but can also endanger the overall safety of the engineering system as well.

Recently, Arif *et al.*<sup>34</sup> proposed a preliminary concept of the structural compliance system for a splitter plate that is able to provide a considerable trailing edge noise reduction without any adverse aerodynamic effects and maintain the structural integrity of the overall system. However, the working mechanism of the compliance system responsible for trailing edge noise reduction is not explored. Furthermore, the effectiveness of the method is only tested for a single type of external disturbance, and the effectiveness of the concept is not yet tested for different flow disturbances. In the present study, we utilize the concept of structural compliance for a splitter plate and explore the underlying physical mechanisms responsible for trailing edge noise reduction by comprehensive aeroacoustic–structural analysis through direct aeroacoustic simulation (DAS). The effectiveness of the proposed approach in noise reduction is analyzed by studying two different test cases. In the first case, the boundary layer over the plate is subjected to a weak monochromatic (single-frequency) excitation to produce laminar instabilities; whereas in the second case, the boundary layer is subjected to a weak broadband excitation. For each test case, the system is uniquely designed by mounting multiple compliant

panels based on the flow characteristics of the boundary layer instabilities. For each system, the panels' structural properties are designed such that their natural frequencies under the fluid loading are similar to the natural frequencies of the flow instabilities within the boundary layer. Hence, the panels undergo structural resonance under the influence of natural/introduced excitation. The sustained structural resonance acts to absorb the energy of incoming acoustic fluctuation and boundary layer instability before they undergo scattering at the sharp edge. A complete design framework is also developed and presented in this paper. Hence, the system can easily be modified to provide noise reduction at any other flow conditions as well. In the present study, only low Reynolds number flow past the splitter plate is considered which results in the laminar boundary layer over the plate. The system design methodology can be implemented for cases with turbulent boundary layers at higher Reynolds numbers as well.

This paper is organized as follows: Section II describes the formulation of the problem and the numerical methodology adopted in the present study. Subsequently in Sec. III, rationale behind the design of compliance systems is discussed. Subsequently, the results of the high-fidelity DAS calculations are analyzed and presented in Sec. IV.

## II. PROBLEM FORMULATION AND COMPUTATIONAL FRAMEWORK

### A. Problem setup

The setup of the physical problem under consideration follows Problem 2 of Category 4 adopted in the Fourth Computational Aeroacoustics (CAA) Workshop on Benchmark Problems,<sup>34,35</sup> which is a common canonical aeroacoustic problem in many studies of trailing edge noise and its control.<sup>29,30</sup> A baseline two-dimensional compressible mixing layer flow formed by a semi-infinite thin rigid splitter plate is considered with its trailing edge placed at the origin (Fig. 1). For the sake of convenience in analysis, all the variables are considered in their dimensionless forms taking freestream flow properties (velocity  $\hat{U}_\infty$ , density  $\rho_\infty$ , and temperature  $T_\infty$ ) and length  $\hat{L}$  as reference, where the symbols with hat ( $\hat{\cdot}$ ) denote their dimensional quantities. The flow above and below the splitter plate has a freestream Mach number  $M = 0.2$  and Reynolds number  $Re_\theta = 530$  based on momentum thickness  $\theta$ , defined by  $\int_0^\delta u/U_\infty(1 - u/U_\infty)dy$ . The thin splitter plate has a blunt end with thickness  $h = 0.105\delta^*$ , where  $\delta^*$  is the boundary layer displacement thickness defined by  $\int_0^\delta (1 - u/U_\infty)dy$ . Such thin thickness avoids self-noise generation by edge bluntness, which dominates whenever  $h/\delta^* > 0.3$  (Ref. 3) and also supports sufficient mesh resolution for resolving the scattering at the edge.

The core idea of the proposed approach utilizes flow-induced structural compliance of multiple elastic panels mounted on the splitter plate for reduction of trailing edge noise scattering. The structural design of elastic panels and their placement on the splitter plate depend upon the flow characteristics. Their details are discussed in detail in Sec. III.

In the present study, two different practical scenarios are considered where the aerodynamic noise is generated due to flow scattering over a flat plate in the presence of external disturbances/loads. These situations are commonly encountered by different aerodynamic devices operating under different off-design/variable flow conditions and subsequently result in excessive tonal or broadband noise. For the first case (hereafter indicated as C1), a practical situation where the plate experiences a monochromatic disturbance is considered in which a

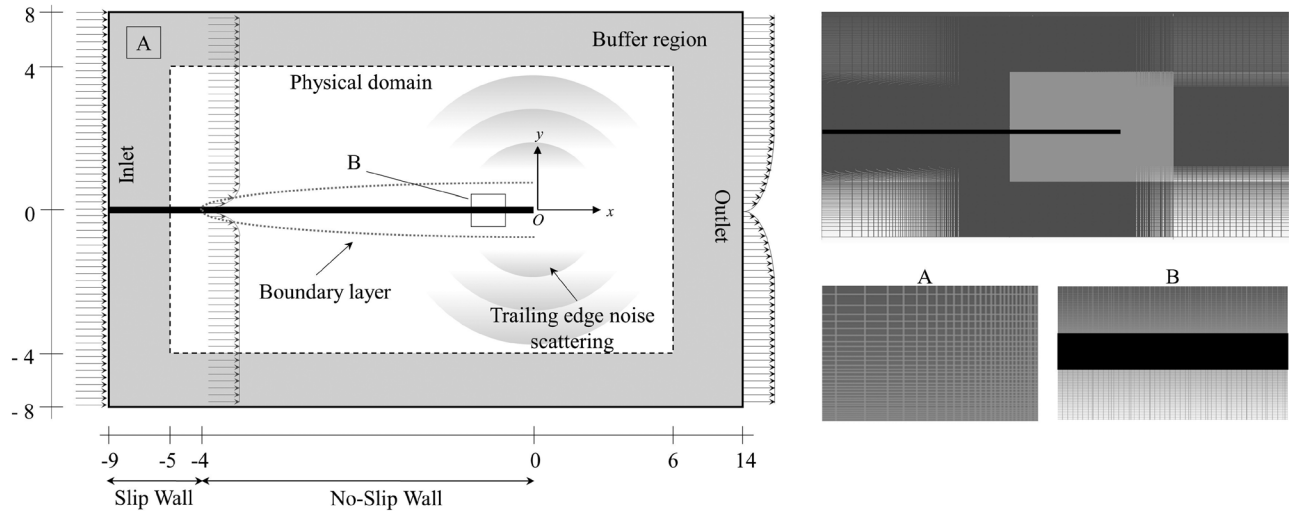


FIG. 1. Schematic sketch of the computational domain (not to scale). Mesh of the complete domain and zoomed views of selected regions A and B are shown on the right.

weak monochromatic acoustic excitation over the upper surface of the plate is set to initiate boundary layer instabilities. These flow instabilities grow while convecting downstream and, subsequently, generate a sharp tonal noise as a result of scattering at the splitter plate trailing edge. For the second case (hereafter indicated as C2), a situation where the plate experiences a disturbance of broadband type, such as gust or interaction of the flow with the surface irregularities, is considered by introducing a weak broadband acoustic excitation over the upper surface. The schematics for both the test cases considered in the present study are shown in Fig. 2.

## B. Numerical methodology

### 1. Aeroacoustical flow solver

The aeroacoustic problem is modeled by compressible N-S equations and the equation of state which govern all the physical aspects of flow dynamics and acoustics. To solve the unsteady equations, the Conservation Element (CE)/Solution Element (SE) scheme is adopted.

It is a robust and highly accurate numerical scheme that enforces strict physical conservation laws in N-S equations in both space and time domains.<sup>36</sup> Details of its implementation are discussed by Lam *et al.*<sup>36</sup> Since its inception, it has been successfully applied to simulate various aeroacoustics problems.<sup>37–40</sup> The two-dimensional N-S equations can be written in a strong conservative form as

$$\frac{\partial \mathbf{U}}{\partial t} + \frac{\partial (\mathbf{F} - \mathbf{F}_v)}{\partial x} + \frac{\partial (\mathbf{G} - \mathbf{G}_v)}{\partial y} = 0, \quad (1)$$

where  $\mathbf{U} = [\rho \quad \rho u \quad \rho v \quad \rho E]^T$ ,  $\mathbf{F} = [\rho u \quad \rho u^2 + p \quad \rho uv \quad (\rho E + p)u]^T$ ,  $\mathbf{F}_v = (1/Re)[0 \quad \tau_{xx} \quad \tau_{xy} \quad \tau_{xx}u + \tau_{xy}v - q_x]^T$ ,  $\mathbf{G} = [\rho v \quad \rho uv \quad \rho v^2 + p \quad (\rho E + p)v]^T$ ,  $\mathbf{G}_v = (1/Re)[0 \quad \tau_{xy} \quad \tau_{yy} \quad \tau_{xy}u + \tau_{yy}v - q_y]^T$ , shear stresses  $\tau_{xx} = (2/3)\mu(2\partial u/\partial x - \partial v/\partial y)$ ,  $\tau_{xy} = \mu(2\partial u/\partial y - \partial v/\partial x)$  and  $\tau_{yy} = (2/3)\mu(2\partial v/\partial y - \partial u/\partial x)$ , heat flux components  $q_x = [\mu/(\gamma - 1)PrM^2](\partial T/\partial x)$  and  $q_y = [\mu/(\gamma - 1)PrM^2](\partial T/\partial y)$ , the Reynolds number  $Re = \hat{\rho}_\infty \hat{U}_\infty \hat{L}/\hat{\mu}_\infty$ , the Mach number  $M = \hat{U}_\infty/\hat{a}_\infty$ , the Prandtl number  $Pr = \hat{c}_{p,\infty}\hat{\mu}_\infty/\hat{k}_{th,\infty} = 0.71$ , total energy  $E = p/\rho(\gamma - 1) + (u^2 + v^2)/2$ , and pressure  $p = \rho T/\gamma M^2$ .

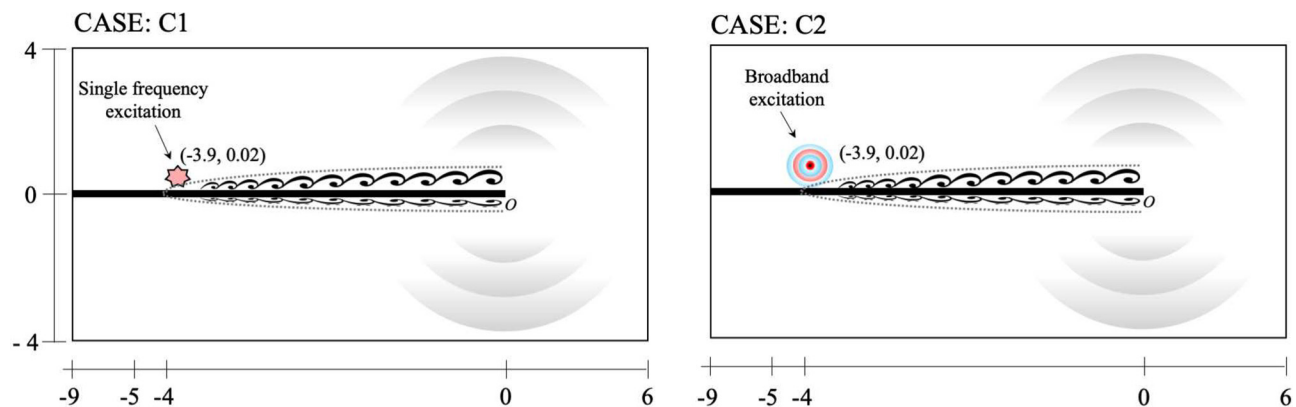


FIG. 2. Schematic representation of the two test cases.

The non-dimensional time and frequency are defined by  $t = \hat{t} \hat{U}_\infty / \hat{L}$  and  $f = \hat{f} \hat{L} / \hat{U}_\infty$ , respectively. The panel length is chosen as the reference length  $\hat{L}$ .

## 2. Structural solver and aeroacoustic/structural coupling

The nonlinear dynamic response of an elastic panel is modeled by solving the one-dimensional plate equation to its simplest approximation.<sup>33,41</sup> The governing equation for panel displacement, normalized by the aforementioned flow reference variables, can be written as

$$S_p \frac{\partial^4 w}{\partial x^4} - (T_p + N_p) \frac{\partial^2 w}{\partial x^2} + \rho_p h_p \frac{\partial^2 w}{\partial t^2} + C_p \frac{\partial w}{\partial t} + K_p w = p_{ex}, \quad (2)$$

where  $w$  is the panel displacement from its undisturbed position,  $S_p$  is the panel bending stiffness,  $T_p$  is the external tensile stress in the tangential direction,  $h_p$  is the thickness of the panel,  $N_p$  is the internal tensile stress in the tangential direction,  $C_p$  is the structural damping coefficient of the panel,  $K_p$  is the stiffness of the foundation supporting the panel, and  $p_{ex}$  is the net pressure acting across panel surfaces.<sup>42</sup> Equation (2) is solved by the standard finite difference method. The nonlinear coupling between aeroacoustic fluctuation and panel structural dynamics is resolved with a monolithic scheme developed by Fan *et al.*<sup>43</sup> In essence, the scheme treats the fluid/panel system as a single entity and includes the effects of panel dynamics on aeroacoustical flow in an extra source term in the CE/SE governing equations [Eq. (1)], which is then solved with a Newton iteration method. The coupling scheme is fully validated with a series of benchmark aeroacoustic-structural interaction problems and is proven to accurately resolve aeroacoustic-structural coupling of increasing complexity.<sup>43,44</sup>

## 3. Computational setup

The computational domain is discretized into a structured mesh composed of  $3400 \times 1200$  mesh elements. The mesh sizes around the splitter plate trailing edge are carefully chosen to achieve minimum spacings of  $\Delta x = 1.9 \times 10^{-4}$  and  $\Delta y = 1.2 \times 10^{-4}$ , so as to ensure there are at least 16 mesh elements across the plate thickness. The mesh is smoothly stretched in the  $x$  and  $y$  directions away from the plate surface. In the application of the CE/SE scheme, a quadrangle mesh element is split into four triangles using diagonal cross divisions.<sup>36</sup> Hence, a total mesh size of  $1.6 \times 10^7$  elements is generated to accurately resolve the flow fluctuations propagating in the proximity of the plate and acoustic propagation to the far-field as shown in Fig. 1. Combined sliding and no-slip boundary conditions are prescribed on all top and bottom plate surfaces. The changeover point between sliding and no-slip conditions on a surface is set to allow the naturally evolving boundary layer to give prescribed  $Re_\theta = 530$  at the plate edge. A buffer zone with exponentially stretched mesh elements is attached to all open physical domain boundaries to avoid any erroneous acoustic reflection. All domain boundaries adopt the nonreflecting boundary condition except the left boundary, which is defined by the inlet boundary condition.

Time-marching of solution to Eq. (1) begins with the steady solution to the compressible boundary layer equations with zero pressure gradient on both sides of the splitter plate with a non-dimensional time step size  $\Delta t = 1 \times 10^{-5}$  to ensure Courant–Friedrichs–Lewy condition (CFL)  $\leq 0.8$ , and its time-stationary solution is taken as the

baseline flow. Every calculation is carried out in a parallel computing facility with 494 CPU cores for a total of approximately 60 000 CPU hours. To analyze the acoustical characteristics required in the present study, 180 virtual probes are placed all with azimuthal increment  $d\theta = 2^\circ$  at radius  $r=3$  from the trailing edge of the splitter plate. Furthermore, 1000 virtual probes have been placed within the boundary layer along the upper and lower surfaces of the plate, respectively, to analyze the aerodynamic behaviors near splitter plate surfaces.

For both cases considered, a weak excitation is introduced to the baseline flow solution, which mainly serves to stimulate the growth of the natural flow instabilities within the boundary layer which are expected to scatter at the splitter plate trailing edge to generate an acoustic wave.<sup>30</sup> The introduced excitation is able to produce an acoustic wave by flow scattering so strong that is almost 40 dB higher than the baseline flat plate (without excitation) in each case. The excitation is modeled as a monopole and introduced at a location  $(x, y) = (-3.9, 0.02)$  on the upper surface splitter plate (Fig. 2). The fluctuating pressure of the excitation is defined as  $p'_{inc} = p_A \sin(2\pi f_{exc} t + \phi_k)$ , where  $p_A = 10^{-5}$  is the constant pressure amplitude and  $f_{exc}$  is the excitation frequency with random phases  $\phi_k$ . For case C1,  $f_{exc}$  is set as 2.78, which matches with the dominant frequency of naturally evolving boundary layer instabilities over the baseline splitter plate (without any excitation). For case C2, the excitation with fluctuating pressure  $p'_{inc} = p_A \sum_{k=1}^{72} \sin(2\pi f_{exc,k} t + \phi_k)$  is introduced in the baseline solution. The broadband excitation frequencies range from  $1.5 \leq f_{exc,k} \leq 5$  with a uniform increment of  $\Delta f_{exc,k} = 0.05$  and random phases  $\phi_k$ . The choice of the range of frequencies allows at least one wavelength of scattered noise at the lowest excitation frequency to be captured within the physical domain and the shortest excitation wavelength to be accurately resolved by the mesh. It is proven in the study by Fan<sup>40</sup> that such form of pressure excitation gives a truly flat excitation spectrum.

## C. Validation of the numerical scheme

The numerical setup is validated by analyzing both the near-field boundary layer characteristics of the rigid splitter plate and acoustic flow field along with their comparison with the literature. Figures 3(a) and 3(b) show the boundary layer profile and displacement thickness growth over the rigid splitter plate for the baseline flow. For comparison, the boundary layer profiles for the baseflow are compared with the analytical solution<sup>45</sup> and the numerical result presented by Visbal and Gordnier<sup>41</sup> at a relatively similar setting with  $M=0.2$  and  $Re_\theta \sim 520$ . The present calculated results are in strong agreement with the literature. All boundary layer profiles follow a similar trend. A maximum deviation of less than 1% is observed between the calculated results and literature. Figure 3(c) shows a snapshot of the instantaneous pressure fluctuations over the rigid splitter plate. The flow instabilities convect over the splitter plate and scatter at the trailing edge to generate acoustic waves. The flow physics for the trailing edge scattering by a splitter plate is qualitatively compared with the trailing edge scattering phenomenon observed by Bae *et al.*<sup>29</sup> for flow conditions of  $M=0.4$  and  $Re_\theta \sim 550$  [Fig. 3(d)]. Good agreement is observed between the flow field plots where the acoustic waves due to trailing edge scattering are generated and propagated upstream with a much higher magnitude than those in the downstream direction. These fluctuations have the same magnitude but opposite signs on each side of the plate. A slight variation in the wavelengths of the trailing edge



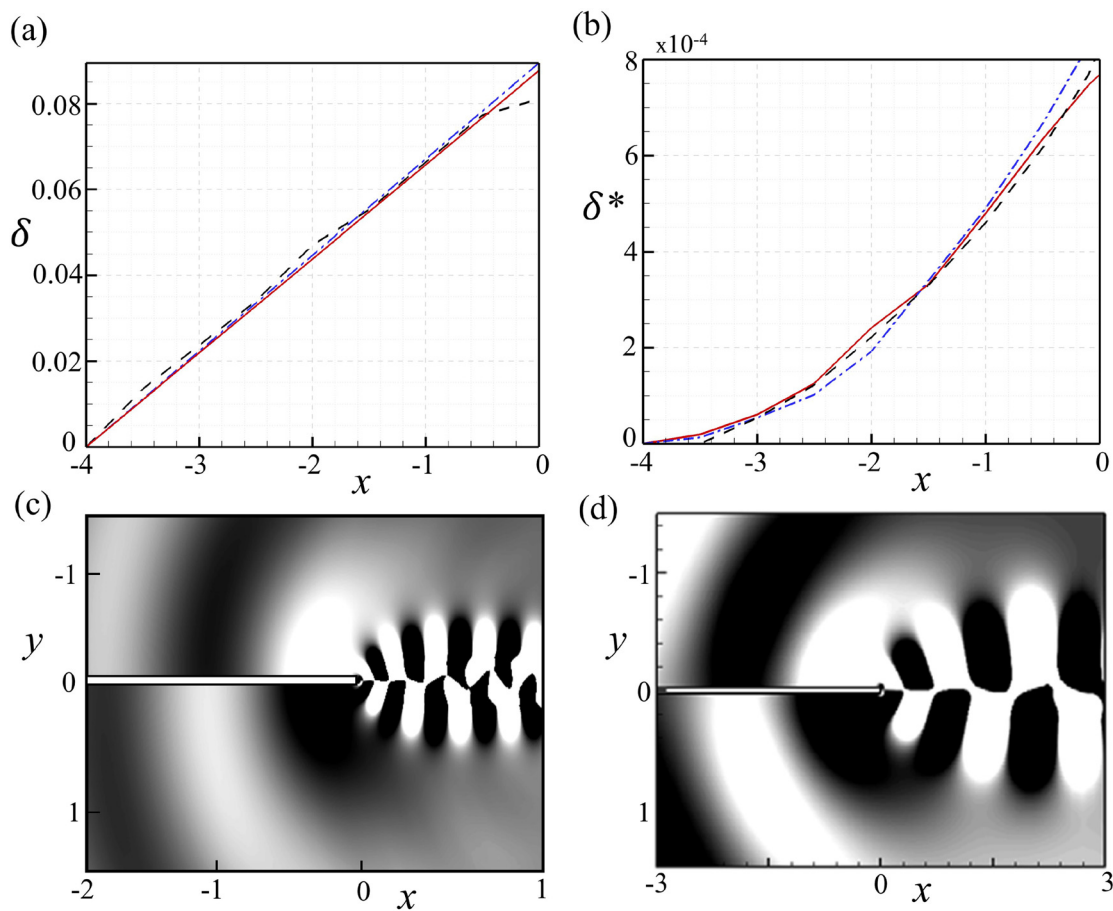


**FIG. 3.** Comparison of boundary layer profiles over the rigid splitter plate. (a) Boundary layer thickness and (b) displacement thickness. Instantaneous pressure fluctuations (40 contours between  $-0.002$  and  $0.002$ ). (c) Present study and (d) Bae *et al.*<sup>29</sup> ---, Present study; -.-.-, analytical solution; —, Visbal and Gordnier.<sup>41</sup>

wake and scattered acoustic waves is observed between the present study and the numerical study in Ref. 29 due to the difference in the freestream Mach number.

### III. DESIGN OF COMPLIANCE SYSTEMS

The design of compliance systems for each case requires certain knowledge of the characteristics of the baseline splitter plate flow from which the identification of possible panel placement locations, panel lengths, and their required structural properties can be ascertained. Hence, the flow behavior within the boundary layer over the surface of the splitter plate is examined first. Arif *et al.*<sup>34</sup> proposed a compliance system design based on multiple elastic panels with their fluid-loaded panel resonant frequencies dependent upon the incoming flow behavior and disturbances. Based on a similar concept, unique compliance systems are designed for the test cases in accordance with the subjected flow excitations. The adopted design methodology is presented in Secs. III A–III C.

#### A. Panel length

In each test case, we utilize elastic panels with length  $L$  equal to  $95\theta$ . Such length of the panel allows interaction between panel

vibration and flow fluctuations with scales comparable to plate boundary layer thickness without distorting the mean splitter plate flow. On the other hand, it is shorter than the dominant wavelength of convective flow fluctuations of the baseline flow  $\lambda_{conv}$  ( $\sim 128\theta$ ) so that the flow-induced vibrating panel would not generate excessive noise.<sup>46</sup> The necessity of the latter criterion was confirmed in a recent study of utilization of flow-induced vibrating panels for airfoil tonal noise reduction.<sup>42</sup>

#### B. Panels location

To ascertain suitable locations for the placement of panels on the splitter plate, the unsteady flow characteristics within the boundary layer on the upper surface of the rigid splitter plate are evaluated for the baseline flow. Figures 4(a) and 4(b) show the fast Fourier transform (FFT) spectra of the transverse velocity fluctuation  $v'$  [where  $v'(x, t) = v(x, t) - v_{mean}(x)$ ] at three different streamwise locations ( $x = -3, -2$ , and  $-1$ ) on the upper and lower surfaces of the rigid splitter plate, respectively. A time episode of non-dimensional time  $t = 10$  with a sampling frequency of  $1 \times 10^5$  is taken, and a Hamming window with no data overlapping is applied. For all the streamwise

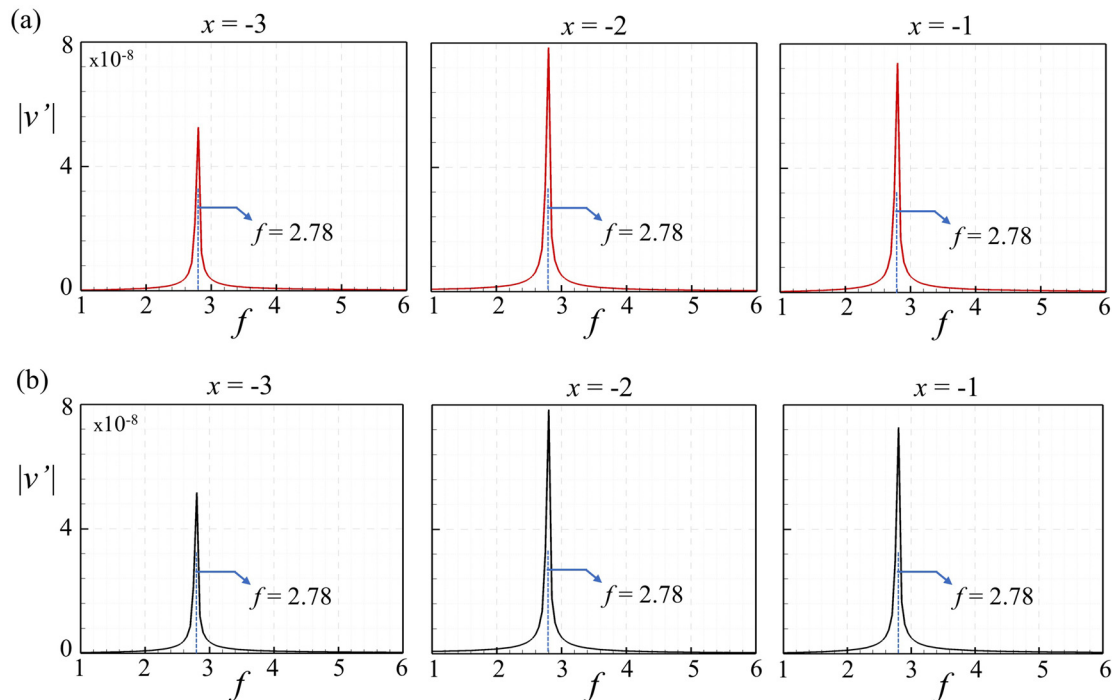


FIG. 4. Spectra of transverse velocity fluctuations at different streamwise locations on the rigid splitter plate. (a) Upper surface and (b) lower surface.

locations, the FFT spectra reveal a sharp peak at  $f = 2.78$  with varying magnitudes. The  $v'$  magnitudes for both the upper and lower surfaces are identical. Hence, only the upper surface of the rigid splitter plate is analyzed in subsequent analyses, unless otherwise specified.

The frequency spectrum of  $v'$  over the complete length of the splitter plate is evaluated to analyze the variations in flow instabilities over the splitter plate. In essence, we take the temporal flow

fluctuations, captured at all locations along the plate surface, through fast Fourier transform (FFT) to obtain their spectral amplitudes, characteristic frequencies, as well as their streamwise distributions. The spectra reveal a dominant fundamental frequency of  $f = 2.78$  within the boundary layer over the complete length of the splitter plate. The variations of the magnitude of  $v'$  along the plate upper surface at the fundamental frequency and its first harmonic are shown in Fig. 5(b).

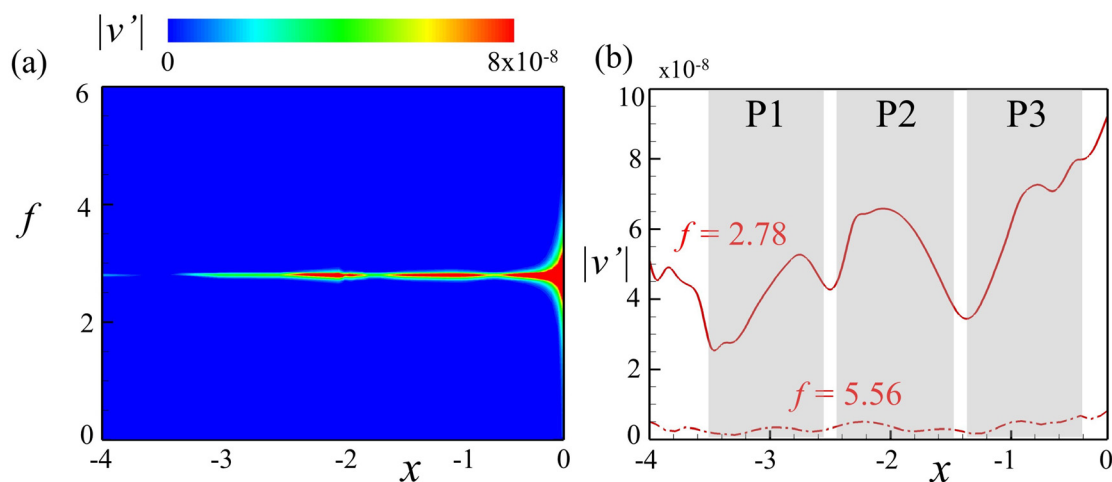


FIG. 5. (a) Distribution of spectrum of transverse velocity fluctuations  $v'$  along the rigid splitter plate upper surface and (b) spatial growth of flow instability over the plate upper surface at the fundamental frequency (solid line) and its first harmonic (dashed-dot line).

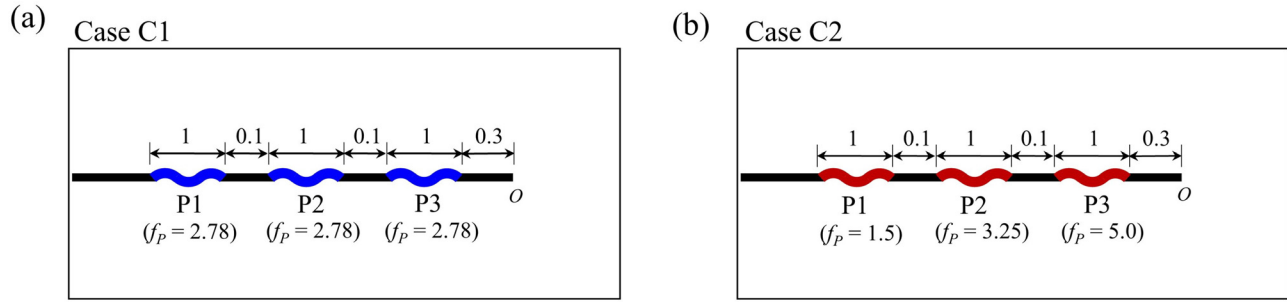


FIG. 6. Panel arrangements for the designed compliance systems. (a) Case C1 and (b) case C2.

The magnitude of the natural boundary layer growth at the fundamental frequency starts to emerge at  $x \sim -3.5$  and exhibits three regions of prominent growth in  $-3.5 \leq x \leq -2.5$ ,  $-2.4 \leq x \leq -1.4$ , and  $-1.3 \leq x \leq -0.3$ . On the other hand, the magnitude of  $v'$  at the first harmonic is much lower than the magnitude at the fundamental frequency. Arif *et al.*<sup>47</sup> exploited an idea of airfoil tonal noise suppression by means of a flow-induced vibrating panel strategically placed on the airfoil suction surface. They found that for optimal noise suppression, the panel leading edge should be placed within the region of sharp spatial growth of boundary layer instability. The same criterion is taken for the placement of compliance systems in the present study. Stemming on the flow characteristics of the splitter plate baseline solution, the designed compliance systems for both cases are composed of three panels (P1 covering  $x = -3.5$ – $-2.5$ , P2 covering  $x = -2.4$ – $-1.4$ , and P3 covering  $x = -1.3$ – $-0.3$ ) separated by  $0.1x$  and are laid at a distance of  $-0.3x$  from the trailing edge, where the edges of each panel are rigidly clamped (Fig. 6).

### C. Panel structural properties

For the elastic panels considered in the present study, the wavelength of the bending waves within the structure is much lower than the convective wavelength of the flow; hence, the fluid would exert an inertial loading on the panel and the natural frequency of the panel would deviate from its *in vacuo* value.<sup>46,48</sup> The panel natural frequency  $f_p$  for resonant mode  $n$  is calculated by including the effect of added mass<sup>49</sup> defined by  $A_m = (\rho_\infty L_p / \pi n)^{-1}$ , and its normalized value can be estimated with the approximation in Ref. 50 as

$$(f_p)_n = \frac{n}{2L_p} \sqrt{\frac{T_p}{\rho_p h_p}} \sqrt{1 + \frac{L_p}{\pi n \rho_p h_p}}. \quad (3)$$

TABLE I. Designed panel parameters.

Case	Panel	Coverage ( $x$ -direction)	Material	Density $\rho_p$	Tension $T_p$	Resonant frequency $f_p$	Resonant mode $n$
C1	P1	$-3.5 \leq x \leq -2.5$	Stainless steel	6367.34	11.1	2.78	2
	P2	$-2.4 \leq x \leq -1.4$	Stainless steel	6367.34	11.1	2.78	2
	P3	$-1.3 \leq x \leq -0.3$	Stainless steel	6367.34	11.1	2.78	2
C2	P1	$-3.5 \leq x \leq -2.5$	Stainless steel	6367.34	3.3	1.5	2
	P2	$-2.4 \leq x \leq -1.4$	Carbon fiber	2212.24	2.6	3.25	3
	P3	$-1.3 \leq x \leq -0.3$	Silicon rubber	833.45	3.1	5.0	3

A key requirement of the proposed compliance system is to select the panel structural properties (density, thickness, and external tension) such that the panel natural frequency coincides with the frequency of the incident flow fluctuations within the boundary layer. For case C1, the design of all three panels (P1, P2, and P3) is identical to provide flow-induced structural resonance at the excitation frequency of 2.78 [Fig. 6(a)]. For case C2, the compliance system is designed with its fluid-loaded panel resonant frequencies increasing along the mean flow direction. The three panels (P1, P2, and P3) for case C2 are uniquely designed to undergo flow-induced structural resonance, respectively, at the lowest frequency  $f = 1.5$ , the middle frequency  $f = 3.25$ , and the highest frequency  $f = 5.0$  of excitation [Fig. 6(b)]. Details of panel properties in the non-dimensional form for both cases are presented in Table I.

## IV. RESULTS AND DISCUSSION

The rigid splitter plate analysis is carried out initially to analyze the effect of excitation on the near-field aerodynamic characteristics and flow scattering at the trailing edge of the splitter plate, which results in acoustic radiation at distant locations. Subsequently, the effect of compliance systems on splitter plate acoustics is evaluated, and the underlying physical mechanisms of noise reduction are explored in detail.

### A. Rigid splitter plate scattering

In every case attempted in the present study, the excitation is turned on and the full solution to Eq. (1) is determined. The effect of introduced excitation for both cases on the trailing edge scattering is analyzed by evaluating the acoustic spectra right above and below the trailing edge of the rigid splitter plate at a radial distance of  $r = 3$  (Fig. 7). For case C1, a sharp peak is observed at the excitation



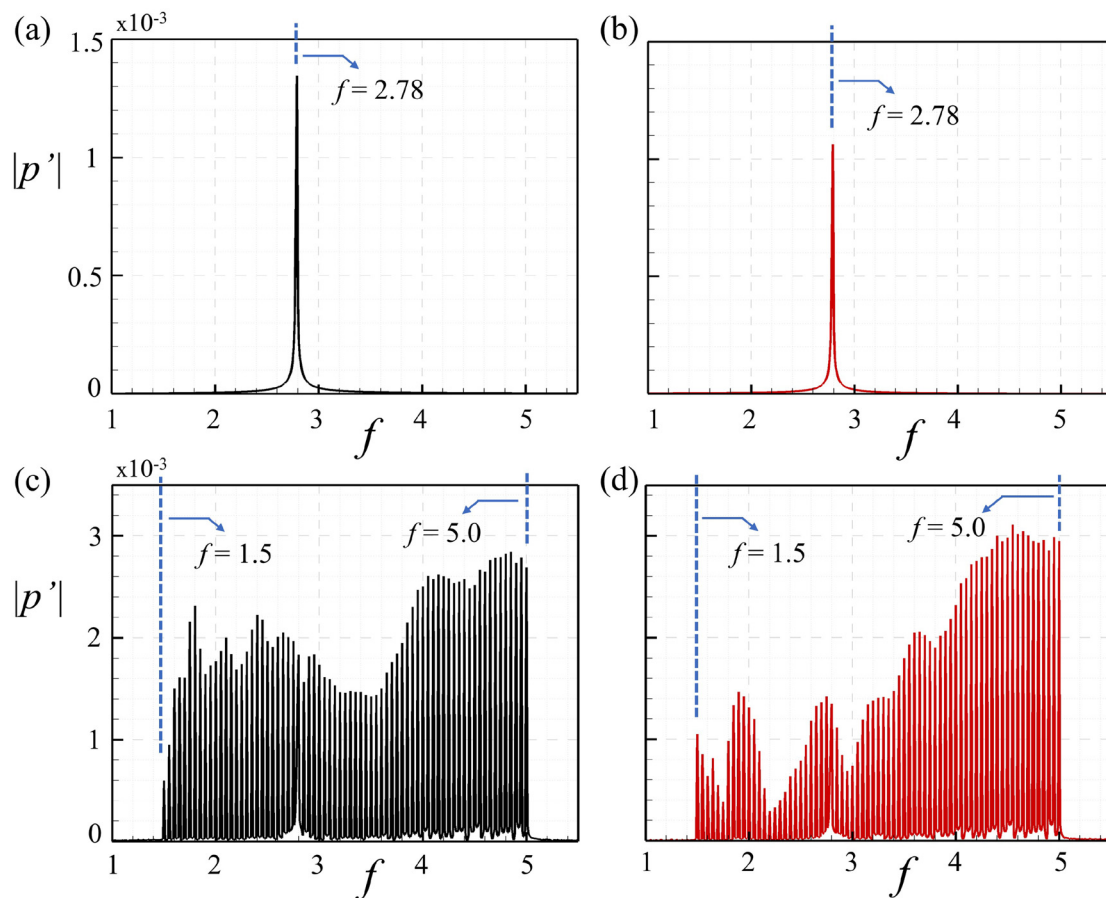


**FIG. 7.** Spectra of scattered acoustic pressure fluctuations at a radial distance  $r=3$  above (left column) and below (right column) the trailing edge of the rigid splitter plate. (a) and (b) Case C1; (c) and (d) case C2.

frequency ( $f=2.78$ ), which confirms the presence of tonal noise due to flow scattering [Figs. 7(a) and 7(b)]. The magnitude  $|p'|$  above the plate is observed to be slightly higher than below the plate. For case C2, the spectral content is widely spread from  $f=1.5-5.0$  with similar magnitudes at lower and mid-range frequencies but greater magnitude at the highest frequency for both above and below the plate [Figs. 7(c) and 7(d)].

The near-field characteristics of the rigid splitter plate flow are analyzed by plotting the frequency spectra of transverse velocity fluctuations  $v'$  within the boundary layer on the upper surface of the rigid splitter plate for both cases. The  $v'$  spectrum for case C1 reveals a dominant fundamental frequency of 2.78, which is similar to the introduced excitation frequency [Fig. 8(a)]. For case C2, the  $v'$  spectrum exhibits a broad range of frequencies similar to the range of excitation frequency ( $1.5 \leq f_{\text{exc},k} \leq 5$ ) [Fig. 8(b)]. The evolution of the  $v'$  magnitude along the plate surface at the characteristic frequencies for both cases is analyzed and shown in Figs. 8(c) and 8(d). For case C1, the variation in  $v'$  magnitude follows a regular pattern which corresponds to the  $\lambda_{\text{conv}}$  for the excitation frequency. For case C2, the variation in  $v'$  magnitude is analyzed for the lowest ( $f=1.5$ ), middle ( $f=3.25$ ), and

highest ( $f=5.0$ ) excitation frequencies. A similar pattern is observed for case C2; however, the magnitude of  $v'$  for  $f=1.5$  is found to be much lower than the other two frequencies.

## B. Acoustic scattering with compliance systems

The scattered acoustic of the splitter plate with both compliance systems are evaluated and compared with that of the fully rigid plate by analyzing their sound pressure level,  $SPL$ , spectra right above and below the plate trailing edge at locations  $(x, y) = (0, \pm 3)$  (Fig. 9). Here,  $SPL = 10 \log_{10}(\bar{p}'^2 / \bar{p}_{\text{ref}}^2)$ , where the reference pressure  $p_{\text{ref}} = 20 \mu\text{Pa}$  is the ISO recommended value for the sound level.<sup>51</sup> For case C1, a reduction of 7.3 dB is observed at the peak tonal frequency above the plate, whereas a reduction of 1.7 dB is observed below the plate [Figs. 9(a) and 9(b)]. For case C2, a fairly uniform 11.1 dB reduction over the entire frequency range of interest is observed above the plate whereas the noise reduction effectiveness below the plate is found to be much lower [Figs. 9(c) and 9(d)].

The azimuth variations of  $p'_{\text{rms}}$  at a radius  $r=3$  from the plate trailing edge are evaluated for both cases. Figure 10(a) shows a

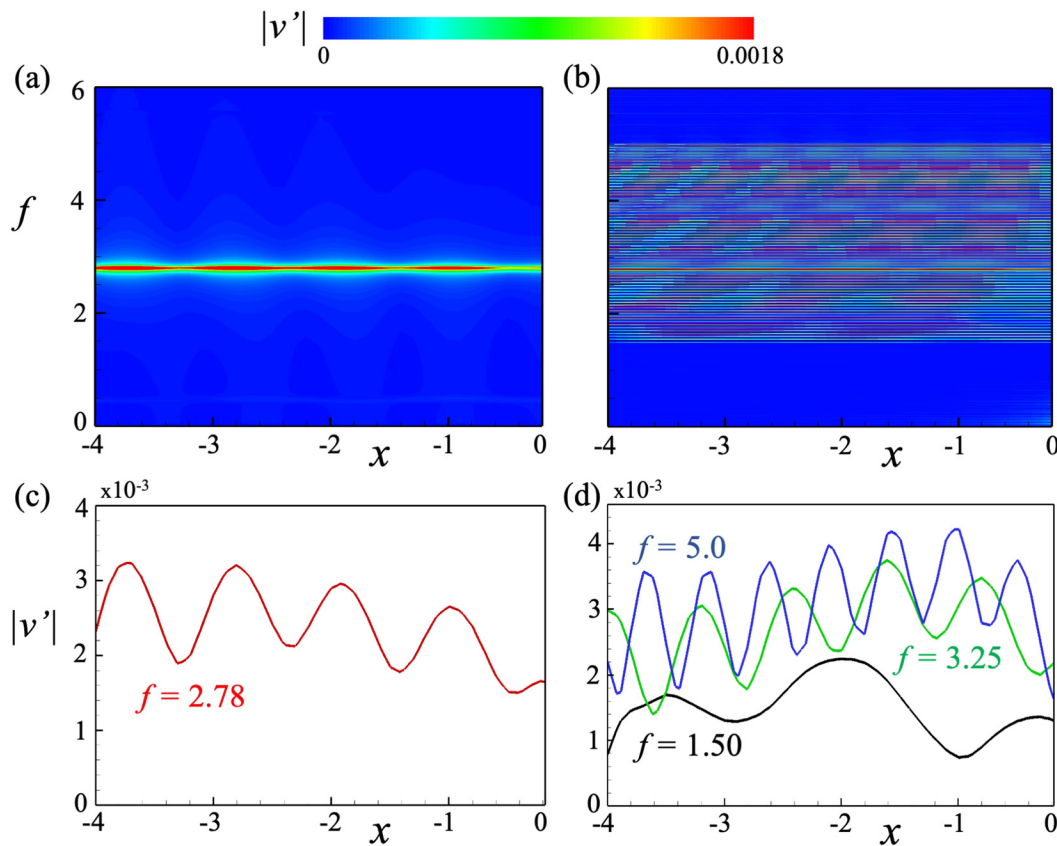


**FIG. 8.** Distribution of spectrum of  $v'$  along the splitter plate upper surface and spatial growth of flow instability over the plate surface at the selected frequencies. (a) and (c) Case C1; (b) and (d) Case C2.

reasonable reduction in acoustic radiation for case C1 by the compliance system where the extent of reduction is observed to be more significant toward the upstream direction. Furthermore, the extent of reduction in  $p'_{rms}$  is observed to be much higher at the azimuth locations above the plate as compared to the lower half. For case C2, a more significant reduction in  $p'_{rms}$  than C1 is observed. Furthermore, a reasonable reduction in  $p'_{rms}$  is also observed at the lower half of the compliance system.

The extent of noise reduction is further illustrated with the reduction in the sound pressure level [ $\Delta SPL_{reduction} = -20 \times \log_{10}(p'_{rms,CS}/p'_{rms,rigid})$ ] at a radius  $r=3$  from the plate trailing edge. The  $\Delta SPL_{reduction}$  for both compliance systems [Figs. 11(a) and 11(b)] show a much higher overall noise reduction above the splitter plate than below where a maximum  $\Delta SPL_{reduction}$  of 15.3 and 15.1 dB is observed above the plate for case C1 and case C2, respectively. For case C1, the noise reduction pattern is observed to be irregular, whereas, for case C2, the noise reduction is observed to be higher at the upstream of the trailing edge with a much regular pattern. The effectiveness of the noise reduction by compliance systems can be illustrated with the change in the sound power level  $\Delta PWL = -10 \times \log_{10}(W_{CS}/W_{rigid})$  in dB, where  $W$  is the integrated sound power for all azimuth locations. A considerable sound power reduction of 4.2 dB is achieved by

case C1, whereas a significantly higher sound power reduction of 7.4 dB is observed for case C2. The physical mechanisms responsible for the observed phenomena for both cases are analyzed in detail in Secs. IV C–IV E.

### C. Linear stability analysis

In order to examine the convective wave instabilities occurring within the boundary layer on the upper surface of the splitter plate, a linear stability analysis is conducted. Additionally, the study investigates how compliance systems can suppress these flow instabilities. The numerical method used for stability analysis in this study is similar to the classical approach commonly employed in the boundary layer transition study, which gives the hydrodynamic stability responses over a base shear flow.<sup>52,53</sup>

The present analysis is based on the evolution of a weak disturbance, which is initiated using information obtained from the time-averaged DAS solution of the rigid splitter plate. The effectiveness and accuracy of this approach have been successfully verified in studies by Arif *et al.*,<sup>42,47</sup> and only a brief overview of its adaptation is provided here. The normalized compressible Navier–Stokes equations in a two-dimensional form, with a constant forcing term  $S$ , can be expressed in a strong conservative form as

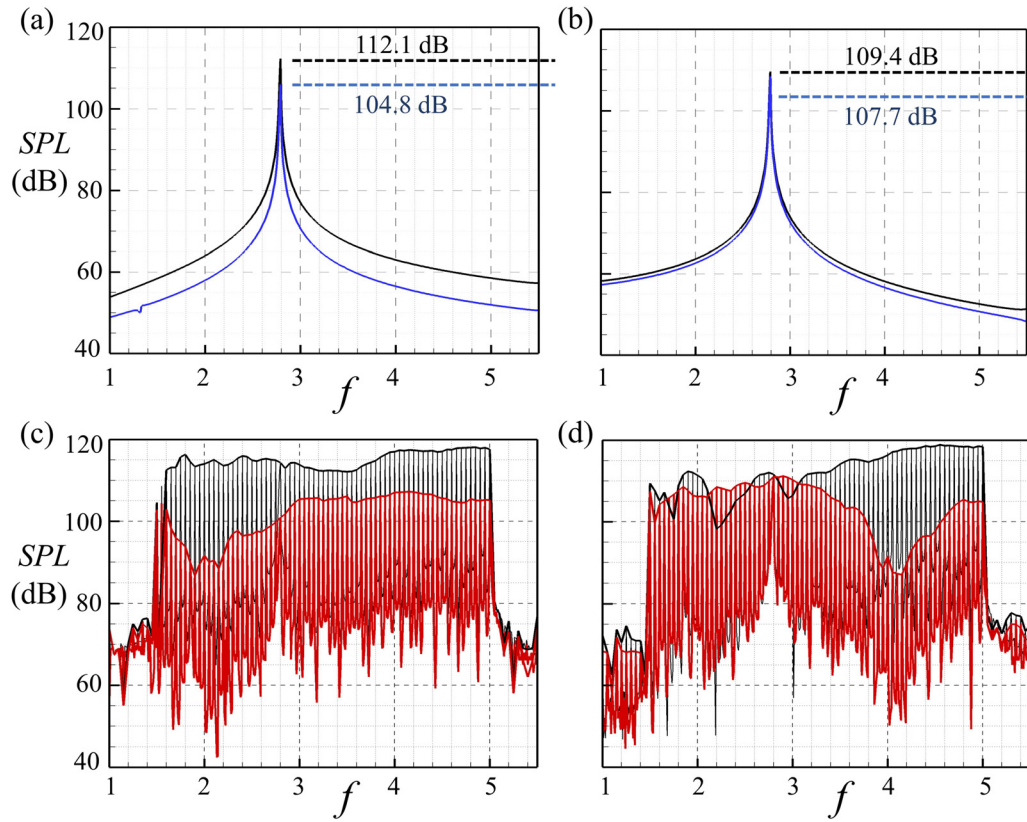


**FIG. 9.** SPL spectra of scattered acoustic pressure at locations  $(x, y) = (0, \pm 3)$ , above (left column) and below (right column). (a) and (b) Case C1; (c) and (d) case C2. —, rigid splitter plate; —, compliance system for case C1; —, compliance system for case C2.

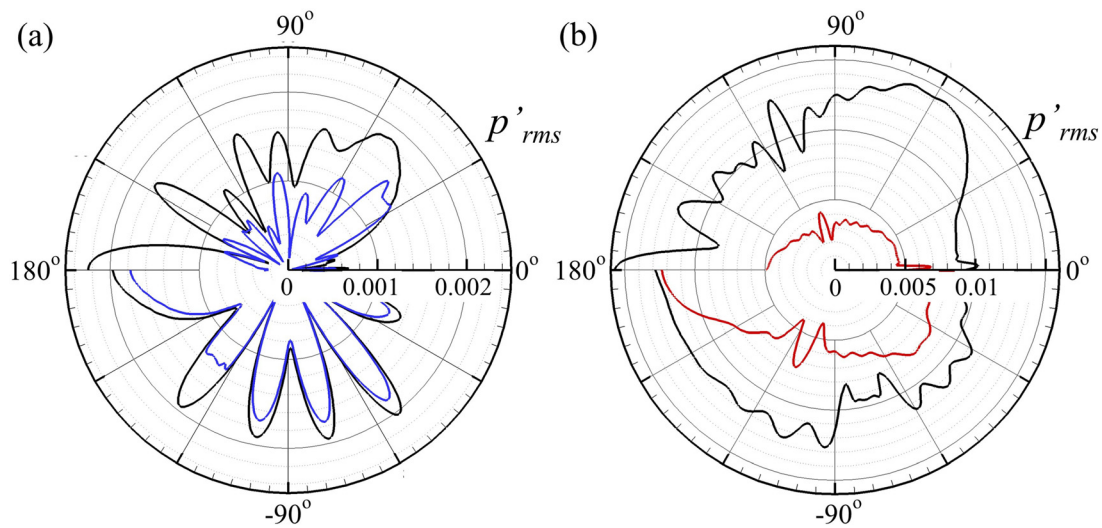


**FIG. 10.** Azimuth distributions of  $p'_{rms}$  at  $r=3$ . (a) Case C1 and (b) case C2. —, rigid splitter plate; —, compliance system for case C1; —, compliance system for case C2.

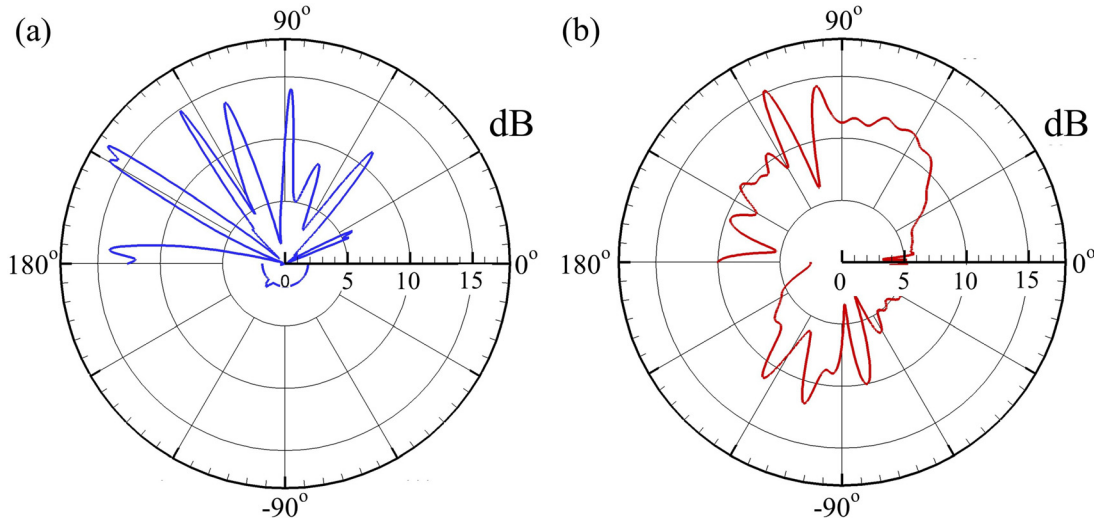


FIG. 11. Azimuth distributions of  $\Delta S_{PL\_reduction}$  at  $r=3$ . (a) Case C1 and (b) case C2. —, compliance system for case C1; —, compliance system for case C2.

$$\frac{\partial \mathbf{U}}{\partial t} + \frac{\partial \mathbf{F}}{\partial x} + \frac{\partial \mathbf{G}}{\partial y} = \mathbf{S}. \quad (4)$$

We may express the unsteady flow in terms of a steady base flow and an infinitesimal perturbation [i.e.,  $\mathbf{U}(x, y, t) = \mathbf{U}_{base}(x, y) + \mathbf{U}'(x, y, t)$ ] and take the forcing term derived from spatial gradients of the base flow, so Eq. (4) becomes

$$\begin{aligned} \frac{\partial(\mathbf{U}_{base} + \mathbf{U}')}{\partial t} + \left( \frac{\partial \mathbf{F}}{\partial x} + \frac{\partial \mathbf{G}}{\partial y} \right)_{base} + \left( \frac{\partial \mathbf{F}}{\partial x} + \frac{\partial \mathbf{G}}{\partial y} \right)' \\ = \mathbf{S} = \left( \frac{\partial \mathbf{F}}{\partial x} + \frac{\partial \mathbf{G}}{\partial y} \right)'_{base} \Rightarrow \frac{\partial(\mathbf{U}_{base} + \mathbf{U}')}{\partial t} + \left( \frac{\partial \mathbf{F}}{\partial x} + \frac{\partial \mathbf{G}}{\partial y} \right)' \\ = \frac{\partial \mathbf{U}'}{\partial t} + \left( \frac{\partial \mathbf{F}}{\partial x} + \frac{\partial \mathbf{G}}{\partial y} \right)' = 0 \end{aligned} \quad (5)$$

as  $\partial \mathbf{U}_{base} / \partial t = 0$ . Note that the homogeneous Eq. (5) has the same mathematical form as the full nonlinear N-S equations but all the primitive variables are replaced by their perturbations in the flux variables  $\mathbf{U}$ ,  $\mathbf{F}$ , and  $\mathbf{G}$ .

To initiate the stability analysis, a broadband disturbance,  $p'_{inc} = p_A \sum_{n=1}^{100} \sin(2\pi f_{exc,n} t + \phi_n)$  is introduced to initiate the calculation, where  $p_A$  is pressure amplitude constant to all frequencies  $f_{exc,n}$  ranging from 0.1 to 10 with a uniform increment  $\Delta f_{exc,n} = 0.1$  and uniformly random phase  $\phi_n$ .<sup>54</sup> A weak  $p_A = 10^{-6}$  is introduced over the upper surface of the plate at a location  $(x, y) = (-3.9, 0.02)$ . When the disturbance propagates into the system interacts with the plate, it generates a wavepacket that travels downstream. This wavepacket has the potential to excite several natural frequencies of the panel. Specifically, at the dominant frequency of the naturally evolving boundary layer disturbance, there is a high likelihood of the occurrence of flow-induced structural resonance. In this condition, the panel would effectively respond and successfully suppress the flow instabilities.

In order to analyze the amplification of instability waves within the boundary layer on the upper surface of the splitter plate, we calculate the wave amplitude function. As the instability wave grows

spatially along the splitter plate, we can consider the wave amplitude as a function that depends on the chordwise location,<sup>4</sup> defined by

$$A(x) = A(x_0) \exp \int_{x_0}^x N(x), \quad (6)$$

where  $N(x)$  represents the spatial growth ratio of the instability wave amplitude.  $A(x_0)$  is the initial amplitude of the instability wave at the reference location ( $x_0 = -3.8$ ), which is just downstream of the initiating disturbance. Since the focus of this study is to analyze the impact of compliance systems on boundary layer instabilities, we evaluate the  $N$ -factor  $N(x) = \ln(A(x)/A(x_0))$  at specific frequencies of interest along the entire length of the plate. This evaluation is done for both rigid and compliant systems to determine the effectiveness of the designed panels in suppressing trailing edge scattering. Figure 12 illustrates the comparison of the  $N$ -factor for both compliance systems with the rigid splitter plate. In case C1, the frequency  $f=2.78$  is selected, while in case C2, three different frequencies ( $f=1.5, 3.25$  and  $5.0$ ) are chosen for the analysis.

In case C1 [Fig. 12(a)], a significant decrease in the  $N$ -factor can be observed for the compliance system across the first two panels (P1 and P2) although the difference in  $N$ -factors between the rigid plate and compliance system becomes smaller over the last panel (P3). Nonetheless, an overall reduction in boundary layer instabilities is still noticeable for the compliance system. In case C2 [Figs. 12(b)–12(d)], a sharp reduction in the  $N$ -factor is evident due to flow-induced panel resonance. At  $f=1.5$ , there is a pronounced decrease in the growth of boundary layer instability over panel P1 ( $x = -3.5$ – $-2.5$ ), as depicted in Fig. 12(b). Although to a lesser extent, a reduction in the  $N$ -factor is also observed over two downstream panels: panel P2 ( $x = -2.4$ – $-1.4$ ) at  $f=3.25$ , and panel P3 ( $x = -1.3$ – $-0.3$ ). A similar phenomenon is observed at  $f=3.25$  [Fig. 12(c)], where the most significant decrease in the  $N$ -factor occurs across panel P2, which is designed to resonate at a similar frequency (i.e.,  $f_p = 3.25$ ). At  $f=5.0$  [Fig. 12(d)], the overall effectiveness of the compliance system in reducing instability growth is diminished.



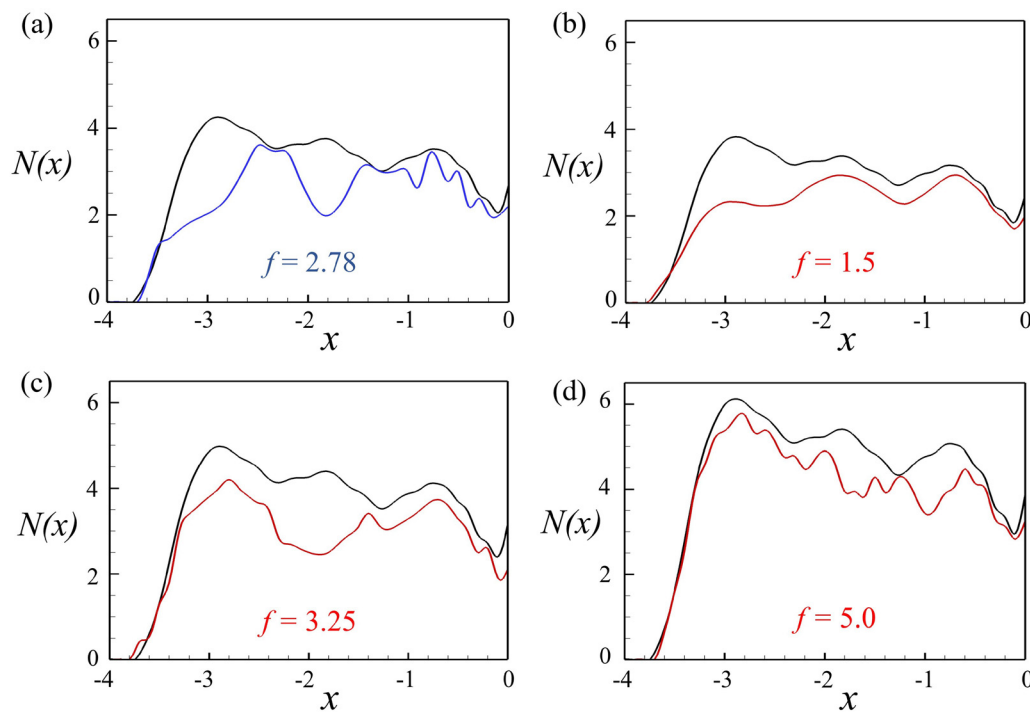


FIG. 12. Streamwise distributions of  $N$ -factor over the upper surface of the splitter plate at the selected frequencies. (a) Case C1; and (b)–(d) case C2. —, rigid splitter plate; —, compliance system for case C1; —, compliance system for case C2.

#### D. Near-field analysis of the compliance systems

Figure 13 compares the streamwise distributions of scattered pressure fluctuations, defined by  $p'$  [where  $p'(x, t) = p(x, t) - p_{mean}(x)$ ], captured on the upper surface of the splitter plate for both cases. In essence, we put the temporal flow pressure fluctuations, captured at all locations along the upper surface of the plate, through fast Fourier transform to obtain their spectral amplitudes for a frequency range of  $1.5 \leq f \leq 5$ , as well as their streamwise distribution. The streamwise distributions for the figure are calculated over a duration of  $t = 10$  with a fine sampling frequency of  $1 \times 10^5$ . For case C1 [Fig. 13(a)], the reduction of the scattered instabilities within the boundary layers by the flow-induced vibration of the first two panels (P1 and P2) is prominent. The effectiveness of the system in suppressing the flow instabilities slightly reduces while convecting over panel P3. This aspect is attributed to the fact that the last panel P3 is subjected to variable fluid loading due to the influence of the fluid-structure interactions of the upstream panels and is not able to absorb the flow energy effectively. This phenomenon is further explored in detail in Secs. IV E 1 and IV E 2. The average reduction in  $p'$  magnitude is also evaluated over the upper surface of the plate as the acoustic wavelength is relatively large such that the complete plate is effectively close to the edge. Figure 13(c) shows that the compliance system for case C1 is able to provide an average reduction of  $\sim 39.8\%$  in  $p'$  magnitude over the upper plate surface [Fig. 13(c)].

For case C2, the reduction of the scattered instabilities within the boundary layers by the flow-induced vibration of the panels is prominent over the entire excitation frequency range. The combined effects from all the panels facilitate the strong overall broadband flow

instability reduction as illustrated in Fig. 13(b). For scattering reduction effectiveness, the compliance system for case C2 gives a significant average reduction in a  $p'$  magnitude of  $\sim 63.4\%$  [Fig. 13(d)]. The high noise reduction might be attributed to different extents of continuous reduction at panel resonant frequencies. These observations show that for a splitter plate under the broadband disturbance, the compliance system should be highly effective when the panel structural resonance at the lowest excitation frequency of interest occurs first in the mean flow direction and subsequently with increasing resonant frequencies.

The contribution of panels for the compliance systems and their effect on momentum fluxes in the flow is investigated by evaluating the time-averaged Reynolds stress  $(\langle u'v' \rangle / U_\infty^2)$  distribution for both compliance systems and shown in Fig. 14. For the rigid splitter plate, the Reynolds stress increases significantly at the trailing edge due to flow scattering, which results in high noise generation. The effect of the compliance systems in suppressing the Reynolds stress is evident for both cases where a prominent reduction in the strength of flow scattering is observed in Figs. 14(b) and 14(d). The magnitude of reduction for the compliance system in case C2 is observed to be much higher than that for case C1.

For a deeper understanding of the effects of designed compliance systems on the trailing edge flow and its acoustic generation, the temporal fluctuations in the pressure fluctuations are FFT-transformed in and, subsequently, filtered for the characteristic frequencies  $(f_{bl})_0$  corresponding to each panel and reconstructed in the whole domain. For the filtered FFT analysis, a total of 10 000 snapshots with a uniform time interval for a time episode of  $t = 10$  are utilized, which correspond to at least 15 cycles of the lowest frequency of interest.



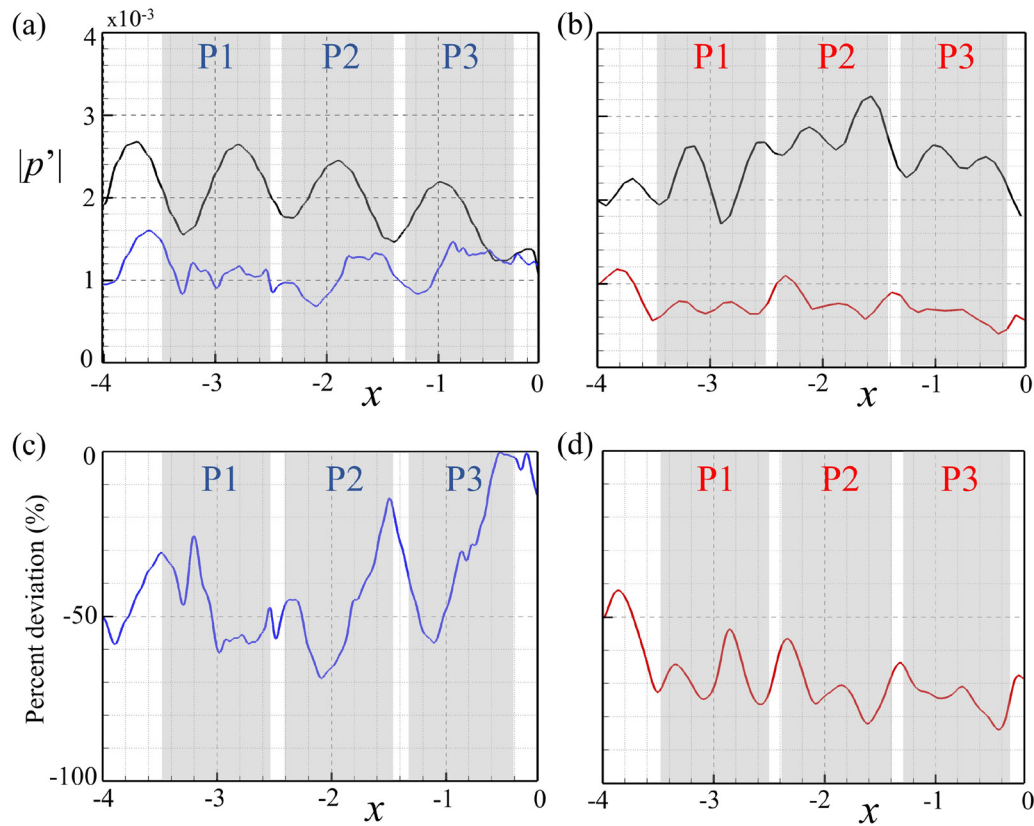


**FIG. 13.** Streamwise distributions of scattered pressure fluctuation magnitudes on the splitter plate upper surface. (a) Case C1 and (b) case C2. Relative deviation in fluctuation amplitudes to the case of the rigid plate. (a) Case C1 and (b) case C2. The shaded areas indicate the coverage of panels. —, rigid splitter plate; —, compliance system for case C1; —, compliance system for case C2.

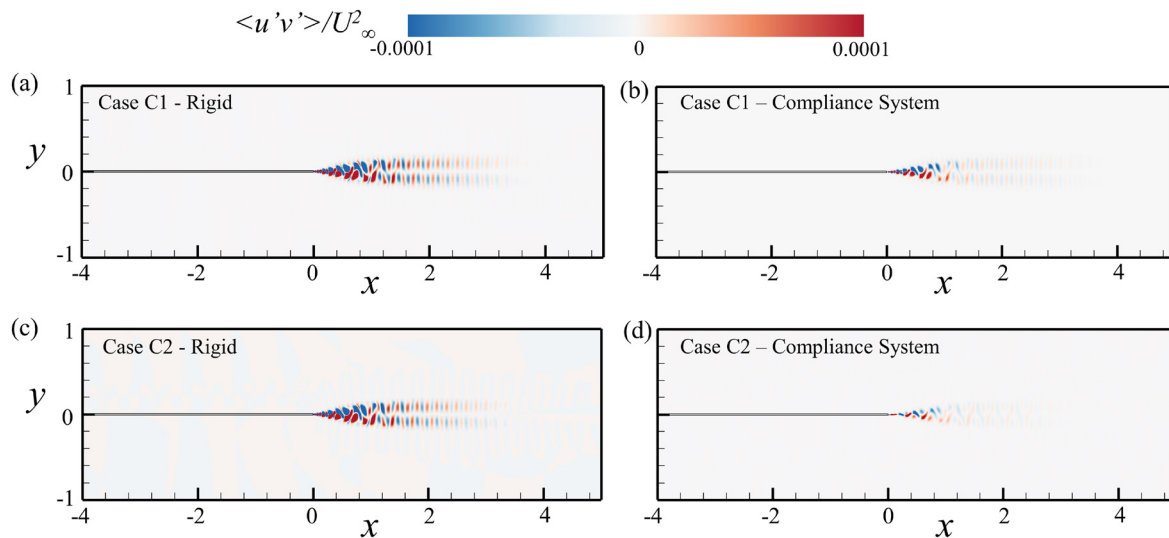


**FIG. 14.** Distribution of time-averaged Reynolds stress over splitter plate without (left column) and with compliance systems (right column). (a) and (b) Case C1 and (c) and (d) case C2.

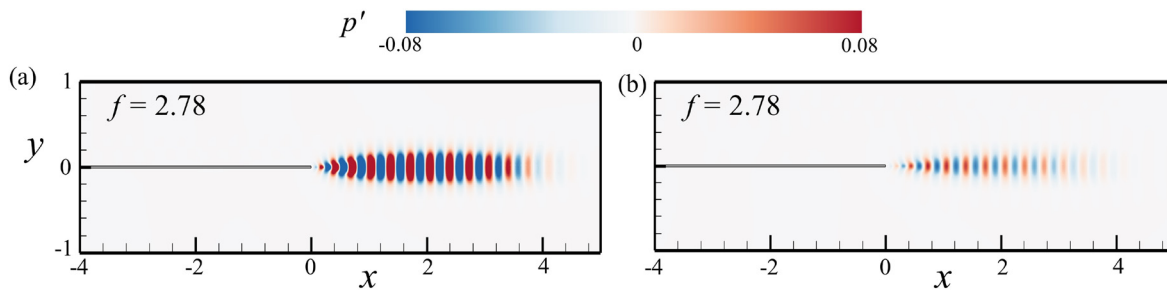


FIG. 15. Filtered FFT magnitude of  $p'$  at  $f = 2.78$  for case C1. (a) Rigid splitter plate and (b) compliance system.

Figures 15(a) and 15(b) correspond to reconstructed filtered  $p'$  flow field data for both the rigid plate and compliance system at  $f = 2.78$  for case C1. It is important to note that for both configurations, the noise generation mechanism is found to be similar where the flow instabilities convect over the trailing edge and scatter as the acoustic wave. A significant difference in the magnitude of  $p'$  can be observed between the rigid and compliance systems. The low magnitude  $p'$  for the designed compliance system indicates that the vibrating panels are able to suppress the flow instabilities over the surface effectively, and as a result, the noise radiation for the compliance system appears to be much weaker than the rigid counterpart.

For case C2, Figs. 16(a)–16(f) correspond to reconstructed filtered  $p'$  flow field data for both the rigid plate and compliance system at  $f = 1.5$ , 3.25, and 5.0, respectively. A noticeable difference in the

reduction of flow instabilities at the trailing edge is observed at each frequency, where the reduction in the magnitude of  $p'$  at  $f = 5.0$  is observed to be much lower than other frequencies. This phenomenon shows that upstream panels P1 and P2 are able to suppress the flow instabilities at their resonant frequencies much more effectively than panel P3, which is subjected to slightly altered flow characteristics due to upstream fluid–structure interactions.

## E. Fluid-panel coupling

### 1. Fluid-panel interface

One of the primary considerations of the compliance system design is to achieve noise reduction without affecting/degrading the splitter plate's aerodynamic characteristics. In this regard, the

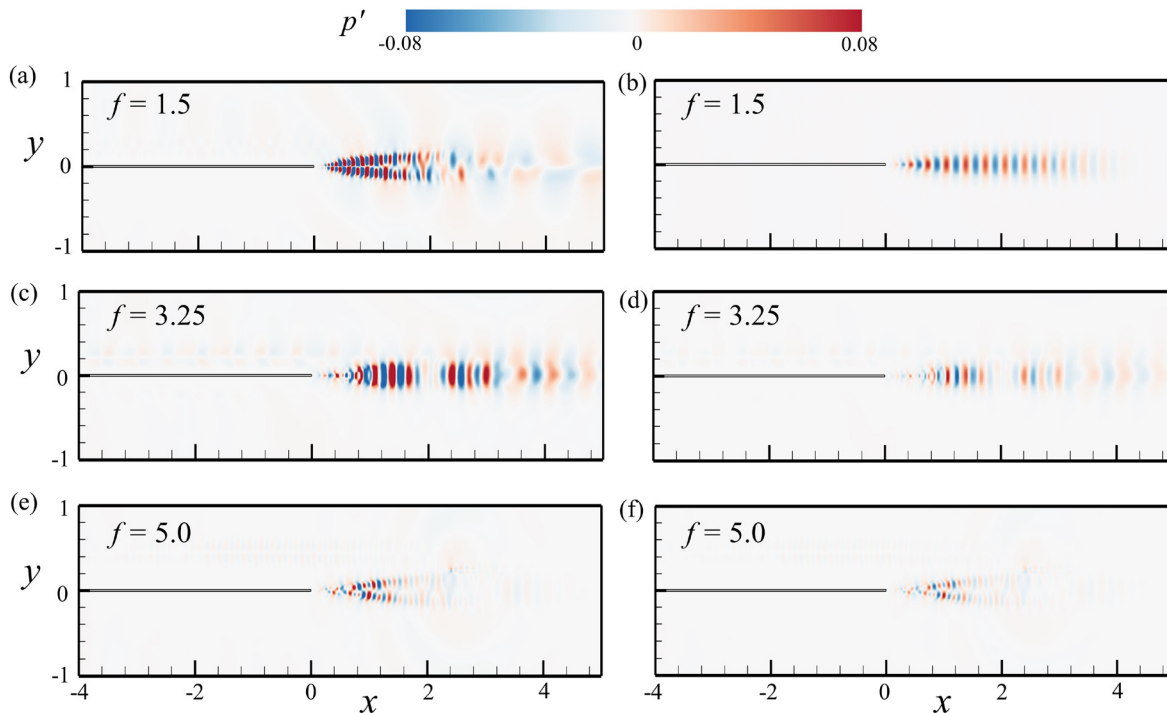
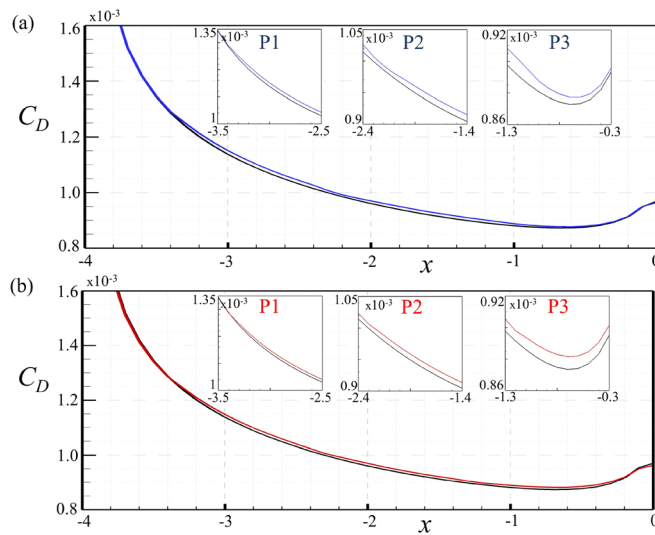


FIG. 16. Filtered FFT magnitude of  $p'$  at  $f = 1.5$  (top row),  $f = 3.25$  (center row), and  $f = 5.0$  (bottom row) for case C2. [(a), (c), and (e)] The rigid splitter plate and [(b), (d), and (f)] compliance system.



**FIG. 17.** Distribution of  $C_D$  over the upper surface of the rigid plate. (a) Case C1 and (b) case C2. The insets in the figures show the zoomed view of  $C_D$  over each panel. —, rigid splitter plate; —, compliance system for case C1; —, compliance system for case C2.

time-averaged coefficient of drag  $C_D$  over the upper surface of the plate is evaluated using 2000 discrete spatial grid points over the plate surface and shown in Fig. 17. The overall  $C_D$  on the upper surface of the plate for both the compliance systems along with their comparison with their rigid counterparts are summarized in Table II. For both cases, the compliance systems maintain the flow characteristics where the maximum deviation of only 0.718% and 0.605% with respect to rigid plate is observed in  $C_D$  for C1 and C2, respectively. The dynamic effect of the panels in compliance systems results in a negligible change in overall drag, which is much lower than the loss of aerodynamic efficiency for a typical fully elastic system ( $\sim 10\%$ – $20\%$ ).<sup>31,32,55,56</sup> The effect of each panel on the  $C_D$  over the upper surface is also analyzed for both cases as shown in insets in Fig. 17. It is evident that upstream panels P1 and P2 do not result in any significant change in  $C_D$ , whereas panel P3 slightly increases the  $C_D$  on the upper surface for both the cases, which is already illustrated in Fig. 13 where the flow-induced vibration of the first two panels (P1 and P2) demonstrates a significant reduction in scattered instabilities within the boundary layers. However, the effectiveness of the system in suppressing flow instabilities convecting over panel P3 slightly diminishes. This phenomenon can be attributed to the more complicated and less harmonious flow, due to complex fluid–structure interactions with the upstream panels, experienced by the last panel P3. Consequently, panel P3 is unable to establish structural resonance in the desired vibration mode shape for effectively absorption of flow energy.

**TABLE II.** Comparison of coefficient of drag  $C_D$  on the upper surface of the plate.

Case	Rigid splitter plate	Compliance system
C1	$1.084 \times 10^{-3}$	$1.091 \times 10^{-3}$ (+0.718%)
C2	$1.084 \times 10^{-3}$	$1.090 \times 10^{-3}$ (+0.605%)

From the acoustic and flow field analyses, it is well ascertained that the designed compliance systems are able to substantially suppress the trailing edge noise without affecting the aerodynamic characteristics. To analyze the effect of panel dynamics on the splitter plate aerodynamics, the time-averaged streamwise boundary layer profiles for both cases are analyzed over the upper surface of the plate at different locations. The locations on the plate are carefully selected to ascertain the impact of panel vibrations on the boundary layer characteristics in its near vicinity with an offset of  $\Delta x = 0.01$  before and after the panel edges. From Figs. 18(a) and 18(b), it is evident that the boundary layer thickness grows along the downstream direction. For both cases, the profiles for rigid and compliance systems are almost identical at all streamwise locations. However, a slight difference is observed in the lower half of boundary layers just downstream from panel P1 up till the trailing edge where the thickness of the boundary layer for compliance systems is slightly reduced and an increase in the near-wall velocity is observed. The reduction in the thickness of the boundary layer for compliance systems ultimately results in less intensive wakes as compared to rigid splitter plate as observed in Fig. 14. The inclusion of compliance systems results in a reduction of approximately 60% in the wake length and around 50% in the angle formed by the wake boundaries from the plate edge. Moreover, the wake momentum deficit are significantly diminished, indicating a notable reduction in the loss of flow dynamic pressure (i.e., pressure drag).

## 2. Panel dynamics

The panel dynamics are examined to uncover the underlying mechanisms responsible for trailing edge noise reduction. Fourier mode decomposition (FMD) analysis<sup>57</sup> is carried out to extract the structural vibration modes of interest and the panel displacement at these modes are analyzed. For FMD analysis, the panel displacement data  $w$  are arranged in a time–space matrix, and FFT is employed to transform it into a frequency–space domain. For case C1, the mode shapes of the panels are extracted by plotting the Fourier amplitude of  $w$  at the first and second modal frequencies  $f_P = 1.39$  and  $2.78$ , respectively [Figs. 19(a)–19(c)]. The mode shapes are easily discernible for all three panels, where the amplitude of the second resonant mode is observed to be much higher than the first mode. The amplitudes  $w$  of the first two panels (P1 and P2) are observed to be higher than the last panel (P3), which indicates that although the panel is vibrating in the desired mode shape, it is still not achievable the maximum displacement. As observed in Fig. 13, this phenomenon results in lower reduction of flow instabilities by panel P3.

For case C2, the modes of the panels are extracted by plotting the Fourier amplitude of  $w$  at the first, second, and third modal frequencies [Figs. 19(d)–19(f)]. All the panels are able to vibrate in the desired resonant modes, i.e., P1 in the second mode, and P2 and P3 in the third mode. Similar to case C1, the last panel (P3) of the compliance system for case C2 also vibrates with a lower amplitude than the other two panels. Nevertheless, the designed panels are truly compliant with fluctuating flow-induced loading of oncoming boundary layer instabilities and are able to vibrate in their desired mode shapes.

Figures 20(a) and 20(b) show the FFT spectra of displacements of panel centers with a sampling frequency of  $1 \times 10^5$ . For both compliance systems, the dominance of the desired structural resonant modes is evident on all the panels (cf. Table I) so the designed frequency coincidence of the compliance system is fully achieved. However, the

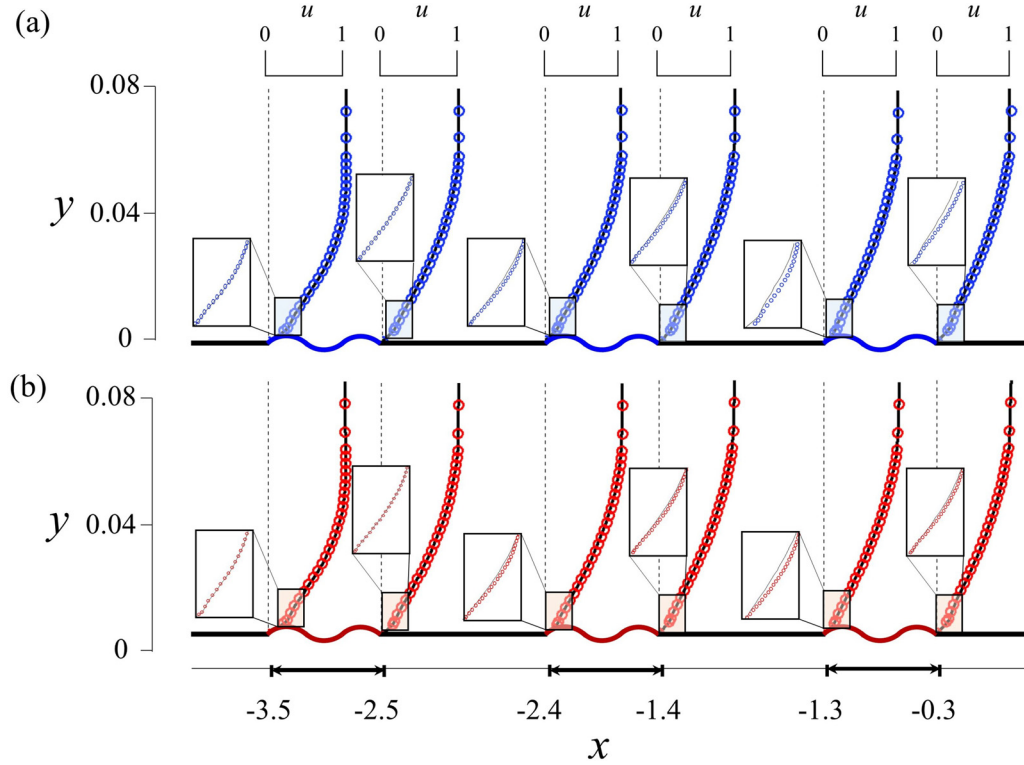


**FIG. 18.** Time-averaged streamwise velocity profiles for rigid splitter plate and compliance systems at different locations. (a) Case C1 and (b) case C2. Black solid line, rigid splitter plate; blue dotted line, compliance system for C1; red dotted line, compliance system for C2.

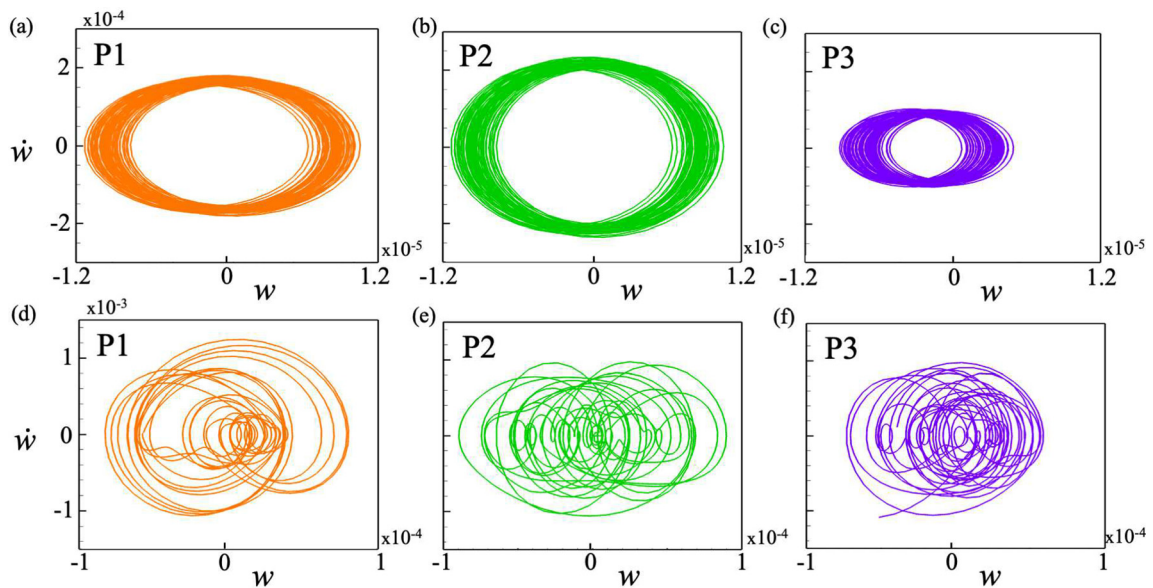


**FIG. 19.** Fourier mode decomposition of the panels displacement. (a)–(c) First two modes of the panels for the compliance system for case C1. (d)–(f) First three modes of the panels for the compliance system for case C2. Dashed–dotted line, first mode; solid line, second mode; and dashed line, third mode. —, P1; —, P2; —, P3.



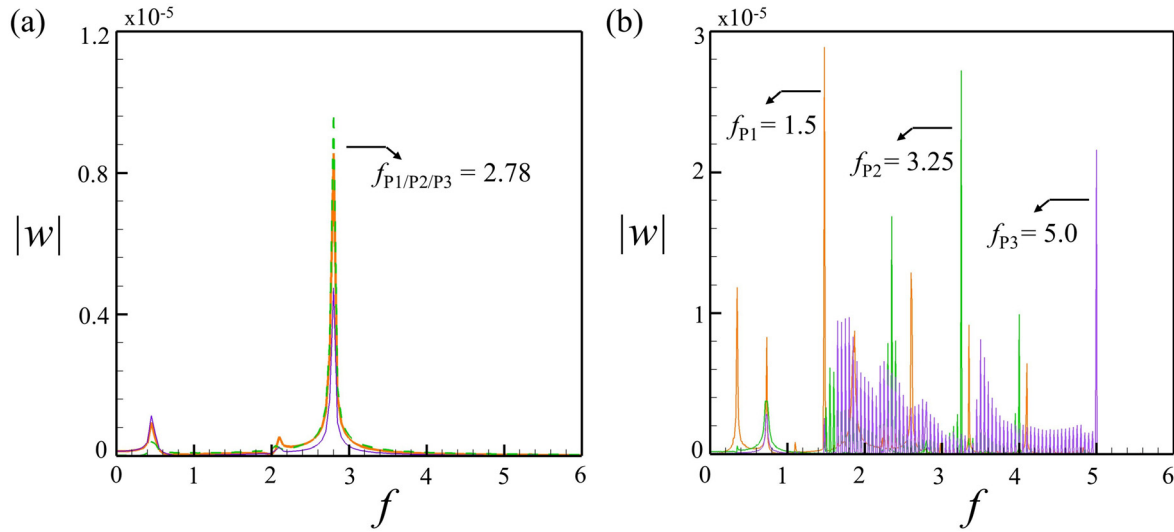


FIG. 20. FFT spectra of panel displacement at the center of panels. (a) Compliance system for case C1 and (b) compliance system for case C2. —, P1; —, P2; —, P3.

displacement amplitude for the last panel for both compliance systems appears to be much lower than the upstream panels, which is in agreement with the observation in Fig. 19.

Although the panel vibratory responses indicate that the desired resonant mode is achieved, it is essential for the panels to sustain their vibrational pattern to effectively absorb the energy from the incident flow. Hence, we analyze the panel phase plane plots with the panel displacement  $w$  and velocity  $\dot{w}$  at the center of the panel<sup>41</sup> (Fig. 21). The phase plane plot for case C1 [Figs. 21(a)–21(c)] clearly indicates that

all the panels have set into sustained limit cycle oscillations with much higher magnitude for P1 and P2 as compared to P3. The panel displacements are observed to be centered around the panel equilibrium position ( $w = 0$ ), which indicates that the panels do not experience any aeroelastic divergence. On the other hand, for case C2 [Figs. 21(d)–21(f)], all the panels show the complex vibrational patterns which ultimately run into sustained into limit cycle oscillations with much higher amplitudes than the panels for case C1. Hence, more energy from the boundary layer is expended to sustain the panel vibrations for the case C2

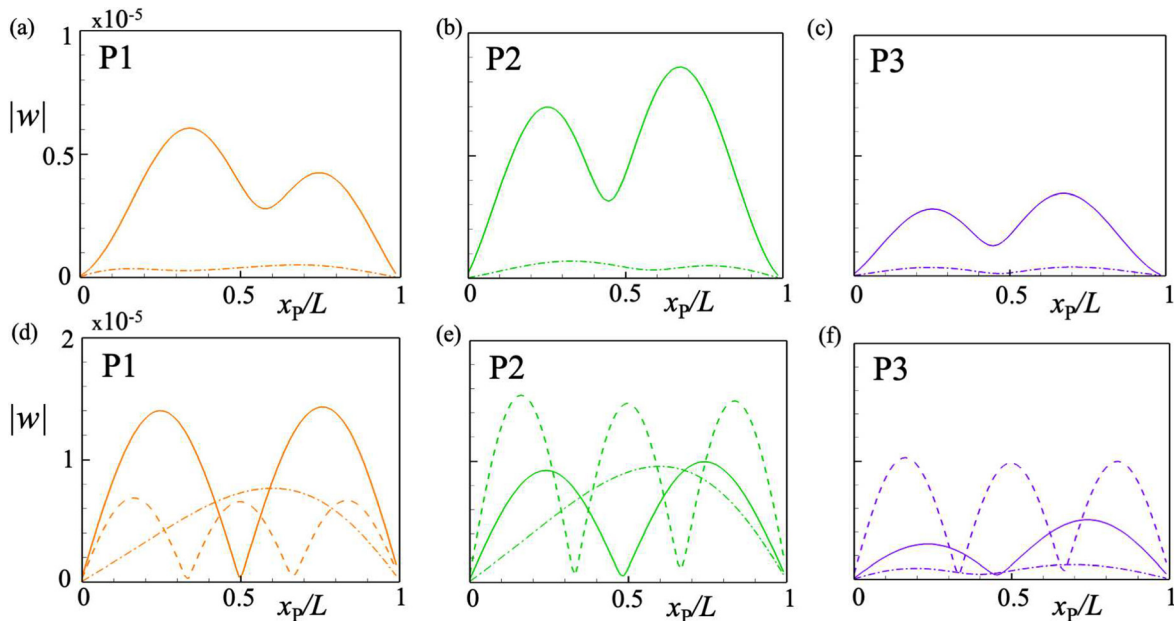


FIG. 21. Phase plots of centers of the panel. (a)–(c) Compliance system for case C1. (d)–(f) Compliance system for case C2. —, P1; —, P2; —, P3.



compliance system which, subsequently, leaves less flow distortion to scatter at the trailing edge for lower noise generation as compared to the case C1 compliance system.

The spatiotemporal evolution of panel displacements for the compliance systems is analyzed and shown in Fig. 22. In every case, the time-stationary solution within a duration of  $t = 3$  is captured in the time synchronized manner for analysis. The spatiotemporal variations of  $w$  for the case C1 compliance system indicate that all the panels are able to maintain the desired second mode and exhibit standing waves [Figs. 22(a)–22(c)]. For the case C2 compliance system, panels P1 and P2 show a more regular standing wave pattern than P3 [Figs. 22(d)–22(f)]. This suggests that a more coherent energy transfer from flow fluctuation prevails over the longer resonant wavelengths of P1 and P2 for sustaining their vibration. The panel displacements of the case C2 compliance system are observed to be much higher than the C1 compliance system. However, it is important to note that for both the compliance systems, the maximum panel displacements are found approximately two orders of magnitude weaker than the local displacement thickness  $\delta^*$  so the mean flow characteristics is effectively unmodified by the vibration of panels.

In order to analyze the correlation between panels vibratory response and their role in noise generation, we perform the acoustic decomposition analysis to estimate the panel acoustic response and its subsequent effects on acoustic reduction by following a similar procedure adopted in earlier DAS studies.<sup>30,58</sup> The acoustic scattering by the

compliance system  $p'_s$ , defined by  $p'_s = p'_r + p'_p$ , is decomposed into the sum of acoustic scattering by rigid splitter plate ( $p'_r$ ) with external acoustic excitation and additional acoustic contribution due to panels vibration ( $p'_p$ ) in isolation (without acoustic excitation). The  $p'_s$  and  $p'_r$  have already been evaluated through DAS simulations. To determine  $p'_p$ , additional temporally synchronized simulations are performed to estimate the radiation by the elastic panels in isolation. In this calculation, the external acoustic excitation is turned off and the elastic panels are forced to vibrate with its vibration velocity time history obtained from the fully coupled DAS solution. Figure 23 shows the time history of pressure fluctuations at a location  $(x, y) = (0, 3)$  right above the trailing edge of splitter for both compliance systems. For case C1 [Fig. 23(a)], acoustic pressure fluctuations due to panels vibrations  $p'_p$  (blue dashed-dot line) are found to be completely out of phase with the  $p'_r$  with a relatively low magnitude. This phenomenon indicates that the panel dynamics counteracts the acoustic field due to flow scattering by the splitter plate. The sum of the two acoustic fields ( $p'_r$  and  $p'_p$ ) eventually results in the reduction of the total acoustic scattering by the compliance system as compared to the rigid splitter plate. A similar phenomenon is observed for case C2 [Fig. 23(b)] with different extent of mutual cancelation effects and amplitudes due to complex panel dynamics.

The relationship between flow dynamics and noise generation is explored by performing the coherence analysis between the  $p'$  signal at  $(x, y) = (0, 3)$  above the trailing edge and  $v'$  signal along a streamline

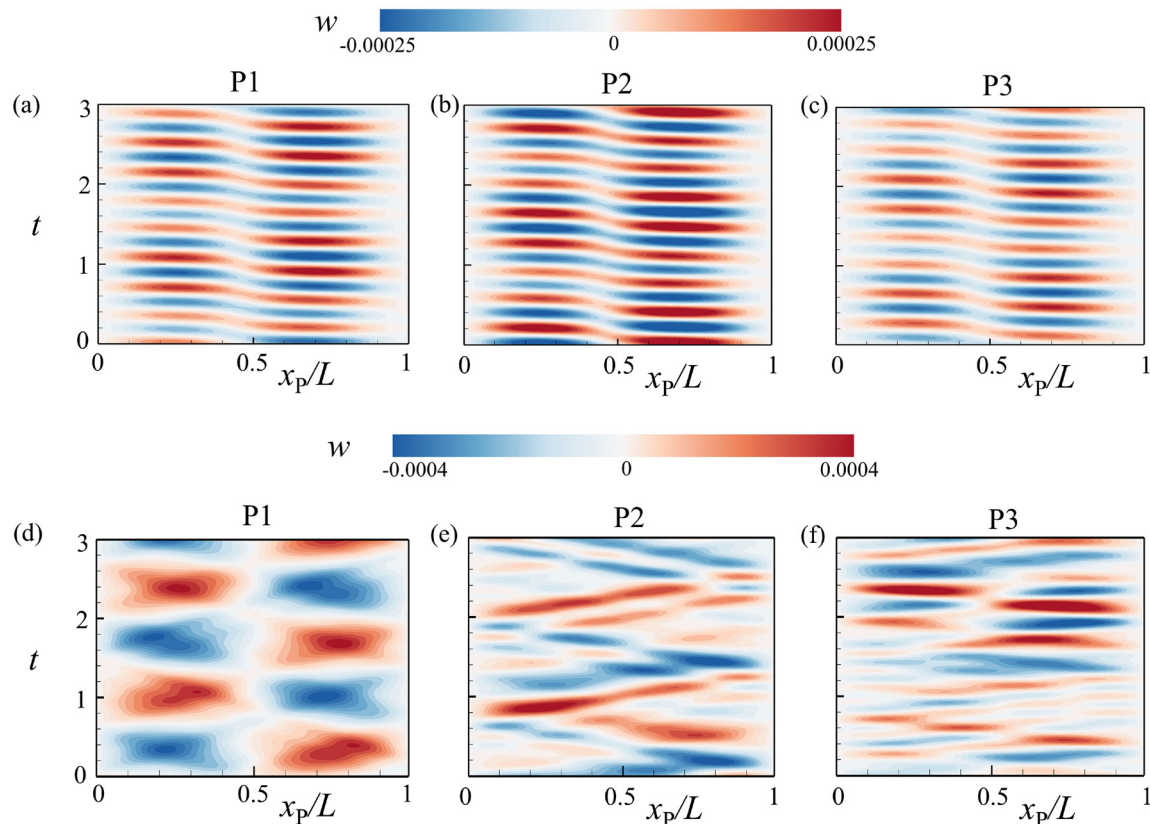
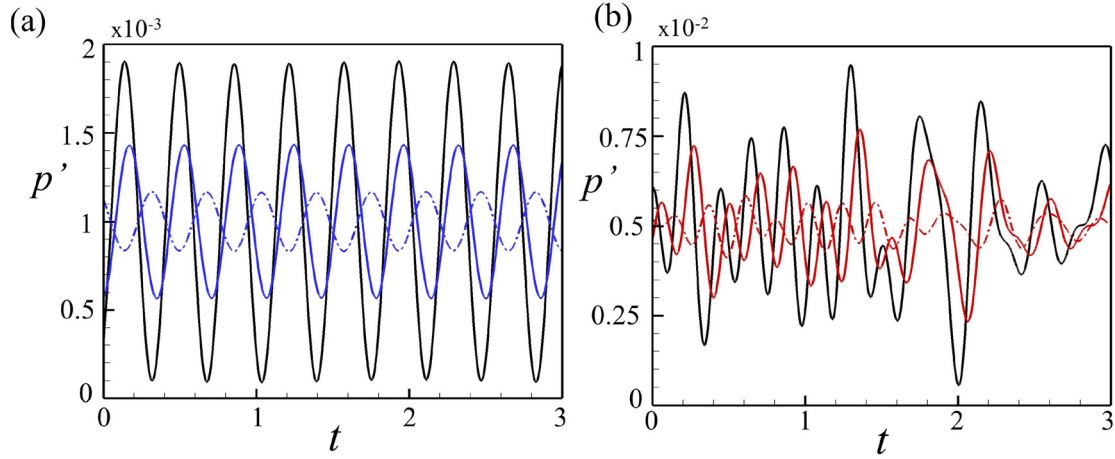
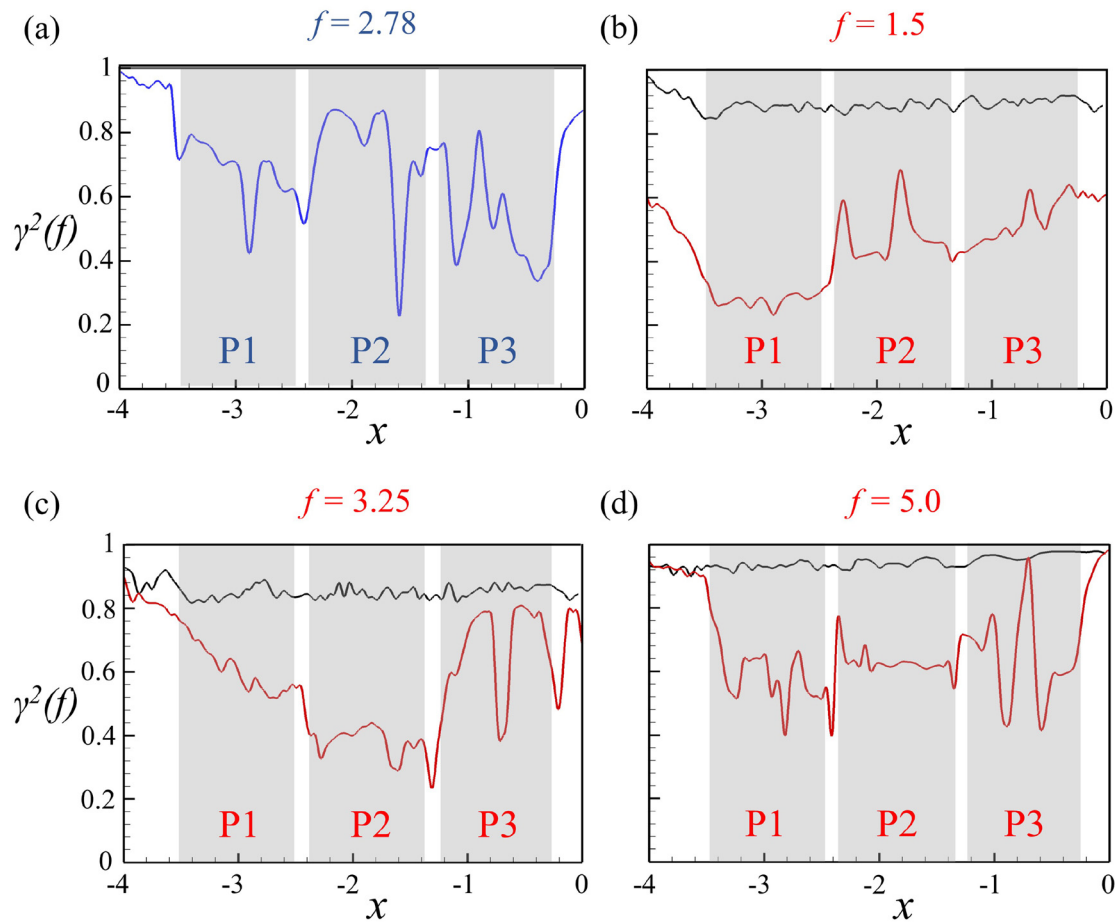


FIG. 22. Spatio-temporal evolution of panel vibration. (a)–(c) Compliance system for case C1. (d)–(f) Compliance system for case C2.  $x_p$ , distance from the panel leading edge.



**FIG. 23.** Acoustic decomposition of scattered pressure fluctuations evaluated at a radial distance  $r=3$  above the trailing edge of the rigid splitter plate. (a) Case C1 and (b) case C2.  $p_s$  represented by solid blue/red line;  $p_r$  represented by solid black line; and  $p_t$  represented by blue/red dashed-dot line. —, rigid splitter plate; —, compliance system for case C1; —, compliance system for case C2.



**FIG. 24.** Magnitude-squared coherence  $\gamma^2_{12}(f)$  plot at the selected frequencies. (a) Case C1 and (b)–(d) case C2. The shaded areas indicate the coverage of panels. —, rigid splitter plate; —, compliance system for case C1; —, compliance system for case C2.

over the upper surface of the splitter plate which is divided into 1000 segments. Figure 24(a) illustrates the  $\gamma_{12}^2$  extracted at  $f=2.78$  for case C1. A high coherence ( $\geq 0.99$ ) between the acoustic and velocity signals is observed for the rigid splitter plate. For the compliance system, a high coherence is maintained up to the first panel P1 leading edge and significantly drops to a minimum  $\gamma_{12}^2 \sim 0.4$  over P1. At panel P2, the  $\gamma_{12}^2$  jumps back to  $\sim 0.82$  at the panel leading edge and drops to a minimum  $\gamma_{12}^2 \sim 0.24$  toward the trailing edge. The  $\gamma_{12}^2$  fluctuate over the panel P3 at an average value of  $\sim 0.52$ . The remarkable reduction in the  $\gamma_{12}^2$  for the compliance system shows that the designed panels are able to effectively reduce the coherence among the flow instabilities and influenced the acoustic generation by the splitter plate.

Figures 24(b)–24(d) illustrate the  $\gamma_{12}^2$  extracted at  $f=1.5$ , 3.25, and 5.0 for case C2. At  $f=1.5$ , a significant reduction in  $\gamma_{12}^2$  is observed at panel P1 as compared to other two panels. Similarly, at  $f=3.25$ , panel P2 is found to be more effective in the reduction of  $\gamma_{12}^2$ . At  $f=5.0$ , no significant change in  $\gamma_{12}^2$  is observed for panel P3 as compared to the other two panels. Overall, the coherence plots for case C2 indicate that the panels at their respective resonant frequencies are more effective in noise reduction as compared to off resonance conditions. However, the panels not only resonate to absorb the flow energy at their designed frequencies but also absorb energy at other frequencies as well [Figs. 24(b)–24(d)]. The combined effects from all the panels facilitate the strong overall noise reduction as illustrated in Fig. 11.

## V. CONCLUSIONS

An approach for controlling the trailing edge noise due to flow scattering at the trailing edge of a semi-infinite thin splitter plate at low Reynolds number flow is proposed. The designed approach utilizes the structural resonance of three rigidly clamped elastic panels under the fluid loading to suppress the flow instabilities within the boundary layer over the plate and reduce the overall trailing edge noise scattering. The effectiveness of the proposed approach is studied using high-fidelity direct aeroacoustic simulation for two different cases. In the first case, a monochromatic acoustic excitation is introduced within the boundary layer, and the compliance system is designed with three identical panels that resonate under the fluid loading at the same excitation frequency. A maximum noise reduction of 15.3 dB is achieved. For the second case, a weak broadband acoustic excitation is introduced within the boundary layer, and the system is designed with three unique panels that undergo flow-induced structural resonance at the lowest frequency, the mean frequency, and the highest frequency of excitation, respectively. A maximum noise reduction of 15.1 dB is achieved. The results of comprehensive aeroacoustic analysis of both compliance systems indicate that the panels are able to maintain the desired mode shapes and exhibit standing waves, which allow a coherent energy transfer from flow fluctuations to sustain their vibration. The proposed approach is not only confirmed feasible with monochromatic and broadband scattering but does not lead to any increase in drag of the plate flow. Given the high noise suppression and foreseen advantages, it is envisaged that the outcomes reported would foster further analytical and experimental studies in the short future.

## ACKNOWLEDGMENTS

The authors gratefully acknowledge the support from the Research Grants Council of the Government of Hong Kong Special Administrative Region under Grant No. 15208520. The second

author is grateful to stipend support to his study from the Department of Mechanical Engineering, The Hong Kong Polytechnic University.

## AUTHOR DECLARATIONS

### Conflict of Interest

The authors have no conflicts to disclose.

## Author Contributions

**Irsalan Arif:** Conceptualization (equal); Data curation (equal); Formal analysis (equal); Investigation (equal); Methodology (equal); Software (equal); Validation (equal); Writing – original draft (equal). **Muhammad Rehan Naseer:** Formal analysis (equal); Investigation (equal); Methodology (equal); Validation (equal); Writing – original draft (equal). **Randolph C. K. Leung:** Conceptualization (equal); Formal analysis (equal); Funding acquisition (lead); Project administration (lead); Resources (equal); Supervision (equal); Writing – review & editing (lead). **Shuaib Salamat:** Formal analysis (equal); Investigation (equal); Writing – review & editing (equal).

## DATA AVAILABILITY

The data that support the findings of this study are available from the corresponding author upon reasonable request.

## REFERENCES

- <sup>1</sup>N. Curle, "The influence of solid boundaries upon aerodynamic sound," *Proc. R. Soc. London, Ser. A* **231**, 505–514 (1955).
- <sup>2</sup>M. Howe, "On the generation of sound by turbulent boundary layer flow over a rough wall," *Proc. R. Soc. London, Ser. A* **395**, 247–263 (1984).
- <sup>3</sup>T. F. Brooks and T. Hodgson, "Trailing edge noise prediction from measured surface pressures," *J. Sound Vib.* **78**, 69–117 (1981).
- <sup>4</sup>G. Desquesnes, M. Terracol, and P. Sagaut, "Numerical investigation of the tone noise mechanism over laminar airfoils," *J. Fluid Mech.* **591**, 155–182 (2007).
- <sup>5</sup>M. S. Howe, "Trailing edge noise at low Mach numbers," *J. Sound Vib.* **225**, 211–238 (1999).
- <sup>6</sup>L. E. Jones, R. D. Sandberg, and N. D. Sandham, "Direct numerical simulations of forced and unforced separation bubbles on an airfoil at incidence," *J. Fluid Mech.* **602**, 175–207 (2008).
- <sup>7</sup>S. Pröbsting, F. Scarano, and S. Morris, "Regimes of tonal noise on an airfoil at moderate Reynolds number," *J. Fluid Mech.* **780**, 407–438 (2015).
- <sup>8</sup>D. J. Moreau and C. J. Doolan, "Noise-reduction mechanism of a flat-plate serrated trailing edge," *AIAA J.* **51**, 2513–2522 (2013).
- <sup>9</sup>S. K. Singh and S. Narayanan, "Control of airfoil broadband noise through non-uniform sinusoidal trailing-edge serrations," *Phys. Fluids* **35**, 025139 (2023).
- <sup>10</sup>Y.-S. Hu, P.-J.-Y. Zhang, Z.-H. Wan, N.-S. Liu, D.-J. Sun, and X.-Y. Lu, "Effects of trailing-edge serration shape on airfoil noise reduction with zero incidence angle," *Phys. Fluids* **34**, 105108 (2022).
- <sup>11</sup>P. Zhou, Q. Liu, S. Zhong, Y. Fang, and X. Zhang, "A study of the effect of serration shape and flexibility on trailing edge noise," *Phys. Fluids* **32**, 127114 (2020).
- <sup>12</sup>E. Talboys, T. F. Geyer, and C. Brücker, "An aeroacoustic investigation into the effect of self-oscillating trailing edge flaplets," *J. Fluids Struct.* **91**, 102598 (2019).
- <sup>13</sup>A. Kisol and L. J. Ayton, "Aerodynamic noise from rigid trailing edges with finite porous extensions," *J. Fluid Mech.* **836**, 117–144 (2018).
- <sup>14</sup>Z. Deng, Z. Yang, and W.-L. Chen, "Experimental investigation of the flow control over an airfoil with owl-inspired trailing-edge modification: On the material, length, and spacing sensitivity," *Phys. Fluids* **35**, 025135 (2023).

- <sup>15</sup>A. Finez, M. Jacob, E. Jondeau, and M. Roger, "Broadband noise reduction with trailing edge brushes," AIAA Paper No. 2010-3980, 2010, p. 3980.
- <sup>16</sup>T. Smith and C. Klettnner, "Airfoil trailing-edge noise and drag reduction at a moderate Reynolds number using wavy geometries," *Phys. Fluids* **34**, 117107 (2022).
- <sup>17</sup>J. Wang, C. Zhang, Z. Wu, J. Wharton, and L. Ren, "Numerical study on reduction of aerodynamic noise around an airfoil with biomimetic structures," *J. Sound Vib.* **394**, 46–58 (2017).
- <sup>18</sup>P. Zhou, S. Zhong, X. Li, Y. Li, W. Chen, H. Jiang, and X. Zhang, "Broadband trailing edge noise reduction through porous velvet-coated serrations," *Phys. Fluids* **34**, 057112 (2022).
- <sup>19</sup>Y. Shi and W. Kollmann, "Improved delayed detached eddy simulation of a porous wavy trailing edge," *Phys. Fluids* **33**, 055128 (2021).
- <sup>20</sup>J. W. Jaworski and N. Peake, "Aerodynamic noise from a poroelastic edge with implications for the silent flight of owls," *J. Fluid Mech.* **723**, 456–479 (2013).
- <sup>21</sup>A. Cavaleri, W. Wolf, and J. Jaworski, "Numerical solution of acoustic scattering by finite perforated elastic plates," *Proc. R. Soc. A: Math. Phys. Eng. Sci.* **472**, 20150767 (2016).
- <sup>22</sup>L. J. Ayton, "Acoustic scattering by a finite rigid plate with a poroelastic extension," *J. Fluid Mech.* **791**, 414–438 (2016).
- <sup>23</sup>S. A. S. Ali, M. Azarpeyvand, and C. R. I. Da Silva, "Trailing-edge flow and noise control using porous treatments," *J. Fluid Mech.* **850**, 83–119 (2018).
- <sup>24</sup>C. Teruna, F. Avallone, D. Ragni, and D. Casalino, "On the noise reduction of a porous trailing edge applied to an airfoil at lifting condition," *Phys. Fluids* **33**, 055132 (2021).
- <sup>25</sup>D. Crighton and F. Leppington, "Scattering of aerodynamic noise by a semi-infinite compliant plate," *J. Fluid Mech.* **43**, 721–736 (1970).
- <sup>26</sup>M. Howe, "Structural and acoustic noise produced by turbulent flow over an elastic trailing edge," *Proc. R. Soc. London, Ser. A* **442**, 533–554 (1993).
- <sup>27</sup>A. Manela, "Sound generated by a vortex convected past an elastic sheet," *J. Sound Vib.* **330**, 416–430 (2011).
- <sup>28</sup>M. J. Colbrook and L. J. Ayton, "A spectral collocation method for acoustic scattering by multiple elastic plates," *J. Sound Vib.* **461**, 114904 (2019).
- <sup>29</sup>Y. Bae, J. Y. Jang, and Y. J. Moon, "Effects of fluid-structure interaction on trailing-edge noise," *J. Mech. Sci. Technol.* **22**, 1426–1435 (2008).
- <sup>30</sup>M. Nardini, R. D. Sandberg, and S. C. Schlanderer, "Computational study of the effect of structural compliance on the noise radiated from an elastic trailing-edge," *J. Sound Vib.* **485**, 115533 (2020).
- <sup>31</sup>S. Serrano-Galiano, N. D. Sandham, and R. D. Sandberg, "Fluid–structure coupling mechanism and its aerodynamic effect on membrane aerofoils," *J. Fluid Mech.* **848**, 1127–1156 (2018).
- <sup>32</sup>E. Kolb and M. Schaefer, "Aeroacoustic simulation of flexible structures in low Mach number turbulent flows," *Comput. Fluids* **227**, 105020 (2021).
- <sup>33</sup>E. H. Dowell, *Aeroelasticity of Plates and Shells* (Springer Science and Business Media, 1974), Vol. 1, pp. 35–38.
- <sup>34</sup>I. Arif, R. C. K. Leung, and M. R. Naseer, "A computational study of trailing edge noise suppression with embedded structural compliance," *JASA Express Lett.* **3**, 023602 (2023).
- <sup>35</sup>M. D. Dahl, in *Proceedings of the Fourth Computational Aeroacoustics (CAA) Workshop on Benchmark Problems* (NASA Technical Documents, 2004), pp. 25–26.
- <sup>36</sup>G. C. Y. Lam, R. C. K. Leung, K. H. Seid, and S. K. Tang, "Validation of CE/SE scheme in low Mach number direct aeroacoustic simulation," *Int. J. Nonlinear Sci. Numer. Simul.* **15**, 157–169 (2014).
- <sup>37</sup>M. R. Naseer, I. Arif, R. C. K. Leung, and G. C. Y. Lam, "Suppression of deep cavity aeroacoustics at low Mach number by localized surface compliance," *Phys. Fluids* **35**, 056115 (2023).
- <sup>38</sup>I. Arif, G. C. Y. Lam, R. C. K. Leung, and M. R. Naseer, "Distributed surface compliance for airfoil tonal noise reduction at various loading conditions," *Phys. Fluids* **34**, 046113 (2022).
- <sup>39</sup>G. C. Y. Lam and R. C. K. Leung, "Aeroacoustics of NACA 0018 airfoil with a cavity," *AIAA J.* **56**, 4775–4786 (2018).
- <sup>40</sup>K. H. Fan, "Computational aeroacoustic-structural interaction in internal flow with CE/SE method," Ph.D. thesis (The Hong Kong Polytechnic University, 2018).
- <sup>41</sup>M. Visbal and R. Gordnier, "Numerical simulation of the interaction of a transitional boundary layer with a 2-D flexible panel in the subsonic regime," *J. Fluids Struct.* **19**, 881–903 (2004).
- <sup>42</sup>I. Arif, D. Wu, G. C. Y. Lam, and R. C. K. Leung, "Exploring airfoil tonal noise reduction with elastic panel using perturbation evolution method," *AIAA J.* **58**, 4958 (2020).
- <sup>43</sup>H. K. H. Fan, R. C. K. Leung, G. C. Y. Lam, Y. Aurégan, and X. Dai, "Numerical coupling strategy for resolving in-duct elastic panel aeroacoustic/structural interaction," *AIAA J.* **56**, 5033–5040 (2018).
- <sup>44</sup>H. K. H. Fan, R. C. K. Leung, and G. C. Y. Lam, "Numerical analysis of aeroacoustic-structural interaction of a flexible panel in uniform duct flow," *J. Acoust. Soc. Am.* **137**, 3115–3126 (2015).
- <sup>45</sup>F. M. White and J. Majdalani, *Viscous Fluid Flow* (McGraw-Hill, New York, 2006), Vol. 3.
- <sup>46</sup>F. J. Fahy and P. Gardonio, *Sound and Structural Vibration: Radiation, Transmission and Response* (Elsevier, 2007).
- <sup>47</sup>I. Arif, G. C. Y. Lam, D. Wu, and R. C. K. Leung, "Passive airfoil tonal noise reduction by localized flow-induced vibration of an elastic panel," *Aerosp. Sci. Technol.* **107**, 106319 (2020).
- <sup>48</sup>Y. Kerboua, A. A. Lakis, M. Thomas, and L. Marcouiller, "Vibration analysis of rectangular plates coupled with fluid," *Appl. Math. Modell.* **32**, 2570–2586 (2008).
- <sup>49</sup>J. Dugundji, E. H. Dowell, and B. Perkin, "Subsonic flutter of panels on continuous elastic foundations," *AIAA J.* **1**, 1146–1154 (1963).
- <sup>50</sup>I. Arif, G. C. Y. Lam, R. C. K. Leung, and D. Wu, "Leveraging surface aeroacoustic-structural interaction for airfoil tonal noise reduction—A parametric study," AIAA Paper No. 2019-2758, 2019, pp. 2758–2773.
- <sup>51</sup>D. A. Bies, C. H. Hansen, C. Q. Howard, and K. L. Hansen, *Engineering Noise Control* (CRC Press, 2023).
- <sup>52</sup>P. Huerre and P. A. Monkewitz, "Local and global instabilities in spatially developing flows," *Annu. Rev. Fluid Mech.* **22**, 473–537 (1990).
- <sup>53</sup>H. L. Reed, W. S. Saric, and D. Arnal, "Linear stability theory applied to boundary layers," *Annu. Rev. Fluid Mech.* **28**, 389–428 (1996).
- <sup>54</sup>L. E. Jones, R. D. Sandberg, and N. D. Sandham, "Stability and receptivity characteristics of a laminar separation bubble on an aerofoil," *J. Fluid Mech.* **648**, 257–296 (2010).
- <sup>55</sup>R. Galvao, E. Israeli, A. Song, X. Tian, K. Bishop, S. Swartz, and K. Breuer, "The aerodynamics of compliant membrane wings modeled on mammalian flight mechanics," AIAA Paper No. 2006-2866, 2006, p. 2866.
- <sup>56</sup>R. E. Gordnier, "High fidelity computational simulation of a membrane wing airfoil," *J. Fluids Struct.* **25**, 897–917 (2009).
- <sup>57</sup>G. Li, B. C. Khoo, and R. K. Jaiman, "Computational aeroelasticity of flexible membrane wings at moderate Reynolds numbers," AIAA Paper No. 2020-2036, 2020, p. 2036.
- <sup>58</sup>G. C. Y. Lam, R. C. K. Leung, H. K. H. Fan, and Y. Aurégan, "Effect of back cavity configuration on performance of elastic panel acoustic liner with grazing flow," *J. Sound Vib.* **492**, 115847 (2021).